JAAS

Accepted Manuscript

This is an *Accepted Manuscript*, which has been through the Royal Society of Chemistry peer review process and has been accepted for publication.

Accepted Manuscripts are published online shortly after acceptance, before technical editing, formatting and proof reading. Using this free service, authors can make their results available to the community, in citable form, before we publish the edited article. We will replace this *Accepted Manuscript* with the edited and formatted *Advance Article* as soon as it is available.

You can find more information about *Accepted Manuscripts* in the Information for Authors.

Please note that technical editing may introduce minor changes to the text and/or graphics, which may alter content. The journal's standard Terms & Conditions and the Ethical guidelines still apply. In no event shall the Royal Society of Chemistry be held responsible for any errors or omissions in this *Accepted Manuscript* or any consequences arising from the use of any information it contains.

ROYAL SOCIETY OF CHEMISTRY

www.rsc.org/jaas

Effect of small quantities of oxygen in a neon glow discharge

Sohail Mushtaq,*[a] Edward B.M. Steers,[a] Juliet C. Pickering,[b] and Viktoria Weinstein[c]

[a] *London Metropolitan University, North Campus, 166-220 Holloway Road, London, UK*
E-mail: s.mushtaq@londonmet.ac.uk
[b] *Blackett Laboratory, Imperial College, London SW7 2BW, UK*
[c] *Formerly at London Metropolitan University*

Abstract

Many studies have already been carried out on the effect of small quantities of molecular gases (oxygen, hydrogen and nitrogen) in argon analytical glow discharges (GD). We report here the first comprehensive study using small amounts of oxygen in a *neon* GD plasma with copper sample. Whilst neon is too costly for routine use in analytical GD spectrometry, such studies help the interpretation of the excitation and ionization processes taking place in the discharge. In all GD, Penning ionization (PI) of analyte atoms, asymmetric charge transfer (ACT) and Penning excitation (PE) of analyte ions have significant roles in populating excited ionized levels, so the higher energy of the neon metastable states and the higher ionization energy compared to argon have a major effect on the appearance of the copper spectrum. Examples of all these effects for copper ionic lines in neon/oxygen mixtures will be presented. For copper atomic lines, it is observed that the changes (such as enhancement due to change in self-absorption and three body collisional recombination or reduction where neutralization of copper ions is suppressed) in emission yield ratios are more significant when higher oxygen concentrations are used. A clear trend of cascading for neon ionic lines with excitation energies about ~56 eV and ~53 eV could be observed in neon/oxygen mixtures. Excitation of the higher atomic energy levels of copper and neon by neutralization of their ionic ground states is also discussed in this work.

1. Introduction

Over the last two decades, many investigations have been carried out on the effect of small quantities of oxygen in an argon glow discharge (GD). In 1994, Fischer *et al.*[1] studied the effects of the addition of oxygen and nitrogen to argon glow discharges using a few analytical lines and reported considerable intensity changes. Wagatsuma and Hirokawa[2] studied the effects of oxygen in an argon glow discharge using copper as the cathode material; they used oxygen concentrations much higher than those likely from oxide material sputtered in a pure gas. Further investigations have been carried out by Fernández *et al.*[3,4] from the Oviedo group. Bogaerts[5] has developed a hybrid model for Ar/O_2 mixtures in a Grimm-type discharge. Mushtaq *et al.*[6] reported the first multi-line study for oxygen as an impurity in an argon GD using the high resolution vacuum UV Fourier transform spectrometer (FTS) at Imperial College (IC) London and also some comparative studies using both GD Time of Flight Mass Spectrometry (GD-ToFMS) and GD Optical Emission Spectrometry (GD-OES).[7]

On the other hand, previous studies on the effect of small quantities of oxygen in neon GD are very limited.[8-10] So far, there is no detailed investigation in this area. In this paper, we report the first comprehensive investigation using small amounts of oxygen in neon GD. Neon has been extensively used when recording spectra in order to undertake term analysis, *e.g.* Nave *et al.*[11] In 1929, Duffendack and Black[12] used argon, neon and helium for experimental verification of the excitation process for manganese and copper samples. They showed that there were strong multiplets that could be excited in neon but not in argon. Neon has been used as the main gas for laser action in hollow cathode discharges, to populate selectively certain upper laser levels.[13] Charge transfer processes between the Cu atom and Ne ions extensively contribute to these levels. Solanki *et al.*[14] investigated the excitation of ion laser transitions in noble gas mixtures in hollow cathode discharges and reported that the dominant excitation mechanism of noble-gas ions was found to be collisions of the second kind between the ground-state noble-gas ions and neon metastables. Evidence for the role of Penning ionization in very low current (1-5 mA), low pressure (~1 hPa) glow discharges was provided by Hess and Harrison[15] using neon and argon as discharge gases. Using various models Bogaerts and Gijbels have used a mathematical simulation to compare neon and argon as discharge gases in a dc glow discharge.[16] Excitation of iron and chromium spectra in a microwave boosted discharge was reported by Steers and Thorne with argon and neon as the carrier gases.[17] The difference between results obtained for the ionic spectra of iron and chromium confirm the role of charge exchange excitation of iron and show that it is not a significant process for the Cr II spectrum. Leis and Steers[18] used neon as well as argon as the plasma gas for a further study of the properties of a microwave boosted glow discharge.

Whilst any analytical advantages do not compensate for the higher cost of using neon for routine analytical GDS, GD studies using neon help the interpretation of the excitation and ionization processes taking place in the discharge. Thus glow discharge excitation and matrix effects in the Zn-Al-Cu system in neon and argon have been reported by Weiss.[19]

Many other studies of the use of neon in mixed gas GD plasmas can also be found in the literature, particularly by Wagatsuma and co-workers.[20-22] In the above literature review, detailed information is given regarding neon as pure gas or in mixed noble gases in glow discharges; however, by contrast the existing literature on the study of small amounts of molecular gases (H_2, O_2, and N_2) in neon is very limited. Now it is well known that the presence of small amounts of molecular gases in the plasma, possibly arising from the sample itself, can cause major changes in the intensity distribution of the spectral lines of both the sample and the plasma gas and lead to serious analytical errors. These analytical errors may result from discrepancy in crater profiles, fluctuation in the discharge parameters or from changes in emission intensities of many analytical lines commonly used in commercial GDS. If neon as plasma gas is used then these analytical errors may need serious attention as the higher metastable states of neon can dissociate/excite/ionize the impurity gases more efficiently in neon than in argon glow discharges.

The excitation and ionization mechanisms in argon analytical glow discharges in presence of molecular gases are understood to some extent, however, as mentioned above, the previous studies on added molecular gases in neon analytical GD are rather limited. Hodoroaba *et al.*,[23] investigated the effect of small quantities of hydrogen on neon GD using a commercial GD instrument with a small number of pre-selected spectral lines and reported that the intensities of the analytical lines are affected by the presence of hydrogen in different ways than in argon GD. Furthermore, it was also recognized that the hydrogen continuum in the argon plasma is the result of the Penning ionization of H_2 with argon metastable atoms. They used constant voltage and pressure with a 2.5 mm diam. anode tube, rather the "standard" analytical conditions (constant voltage and current with a 4 mm diam. anode tube). Recently Weinstein has repeated their experiments using 700 V and 20 mA with a 4 mm diam. anode tube and recorded similar trends to those observed by Hodoroaba, but differing in magnitude.[24]

We have carried out a comprehensive study for oxygen as an added gas in neon/copper GD, using the IC high resolution vacuum VUV FTS allowing several hundred spectral lines to be investigated over a wide spectral range, including atomic and ionic emission lines of copper and neon. It will be discussed how oxygen can affect existing excitation processes (Penning Ionization, charge transfer & Penning excitation) of ionic levels and the excitation processes of the atomic levels. Examples of all these effects will be presented in the section 3.

2. Experimental Details

The effect of oxygen in neon plasma on the analytical glow discharge was investigated using the equipment previously described,[6] *i.e.* the high resolution vacuum UV Fourier transform spectrometer[25] at Imperial College, London, with a free standing Grimm-type GD source running in dc excitation mode. The plasma gas was supplied to the source *via* a mixing system using three mass flow controllers (MKS Instruments Inc.). For neon as main gas, the pumping speed was restricted by a constriction to reduce the consumption of the gas and a range of oxygen concentrations was obtained by mixing pure neon with pure oxygen. The pressure was measured by a Baratron capacitance diaphragm gauge (MKS Instruments, Inc.), with a pressure range up to 20 Torr, connected directly to the body of the glow discharge source. Considerable pressure changes are needed when oxygen is added in neon to maintain constant voltage (see Table 1). A liquid nitrogen cold trap was installed in the gas inlet line to the source to remove any possible moisture from the gas.

The spectrometer resolution chosen ranged from 0.055 cm^{-1} to 0.033 cm^{-1}. Details are listed in Table 2. In most cases, this was sufficient to resolve the true line profiles allowing spectral line shapes to be observed. Interferograms were recorded, transformed to spectra and analysed as described earlier.[6] Intensity measurement errors are the order of the symbol size for all following figures and supper rate measurements errors are somewhat greater but affect all points similarly. The copper samples (purity 99.5%) (Goodfellow, Cambridge) were 50 mm square with thickness approximately 2 mm. The results presented here were obtained using a 4 mm anode tube with 700 V and 20 mA, 'standard' conditions for GDS analytical work. A constant current dc power supply was used, and the pressure was controlled manually to maintain a constant voltage.

Sputter rate measurements were carried out with the same pure sample plates as used for FTS experiments. Various non-overlapping areas of the sample, circular and 4 mm in diameter, were sputtered for a defined time in the glow discharge source at constant current-constant voltage (20 mA, 700 V). After each replacement of the sample, no gas was admitted into the source until the pressure had fallen below 0.02 Torr. Final evaluation of the sputter rates of samples at various concentrations of oxygen was undertaken by measuring the volume of craters on the sample surface using a Frier Research & Technology (FRT) optical depth profilometer (MicroProf) at Leibniz-Institut für Festkörper- und Werkstoffforschung (IFW) Dresden (Germany).

3. Results and discussion

3.1 Appearance of the copper spectrum in neon and argon glow discharge

Prior to discussing the changes produced by the added oxygen in neon analytical GD, it is useful to describe the various excitation and ionization processes and the appearance of the copper spectrum when two different plasma gases (neon and argon) are used and then to discuss how the presence of oxygen in a neon plasma affects each of these processes. Copper spectra in the 200-300 nm spectral region with pure neon and argon gas are shown in Fig. 1(a) & (b). In addition, the partial energy level diagram of copper is also shown in Fig. 1(c), along with metastable and ionic energy levels of argon and neon. It can be seen that the higher neon metastable states and the higher ionization energy of neon as compared to argon have significant affects on the appearance of the copper spectrum. In the copper spectrum in pure neon plasma, there is a group of Cu II emission lines from the copper ionic energy levels close to the ionization energy of the neon (21.564 eV), which are suitable for asymmetric charge transfer involving neon ions (Ne-ACT), *viz:*

$$Cu_o\ (4s\ ^2S_{1/2}) + Ne^+\ (2p^5\ ^2P_{3/2}) \rightarrow Cu^+* + Ne_o\ (2p^6\ ^1S_0) + \Delta E, \qquad (1)$$

where the subscript $_o$ and superscript * represent ground and excited states respectively, and ΔE is the small energy difference which can be either positive (exoergic) or negative (endoergic).

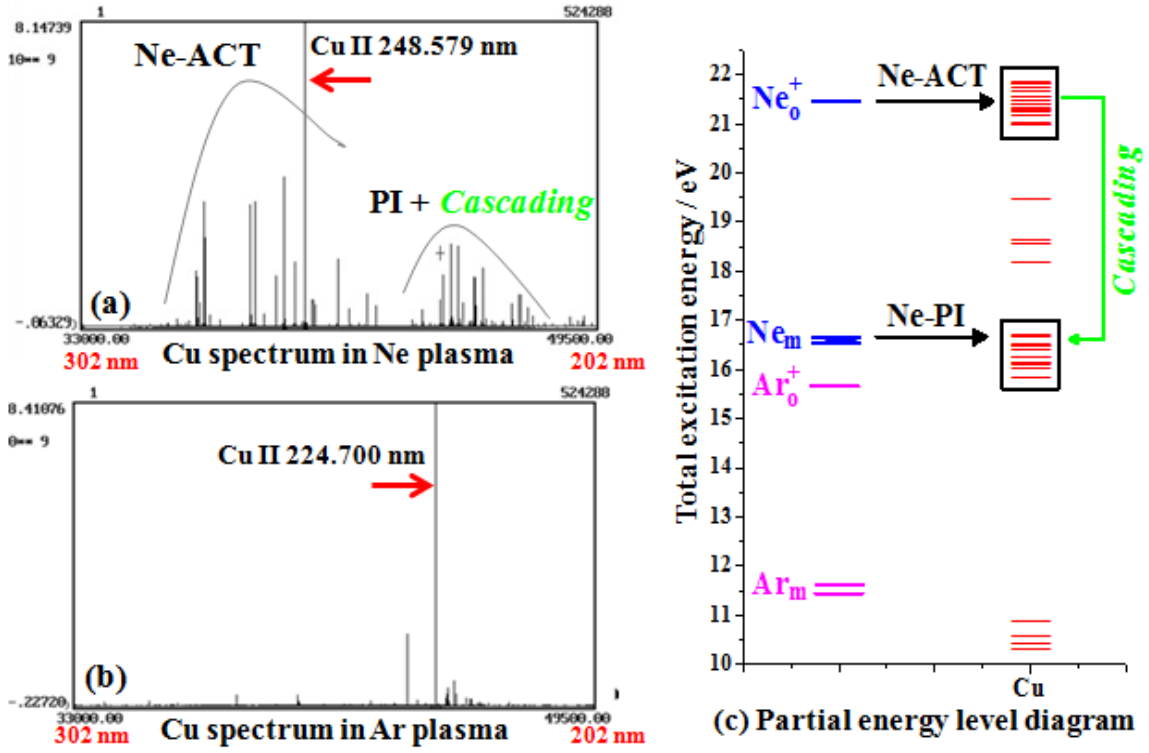

Fig. 1 GD copper spectra recorded with the IC Fourier transform spectrometer using (a) neon and (b) argon as the plasma gas. On right side (c) is a partial energy level diagram of copper ionic states along with metastable and ionic states of argon and neon.

The probability of charge transfer reaction increases when excited levels are close to resonance (*i.e.*, ΔE is very small). In the case of copper as cathode material, we can see in Fig. 1(c), there are many copper ionic energy levels close to the ionization energy of neon, which are suitable for both the exoergic Ne-ACT and endoergic Ne-ACT process. On the other hand, copper does not possess ionic energy levels suitable for Ar-ACT by ground state argon ions, however, there is one Cu II

energy level, 4p $^3P_2$, 15.964 eV, lying close to the argon ionic metastable level and therefore strongly excited by Ar-ACT (Ar_m^+-ACT).[26]

The intense Cu II 224.700 nm line, excited by Ar_m^+-ACT in the copper spectrum in pure argon gas can be seen in Fig. 1(b). In neon GD there are many lines excited by Ne-ACT. There is also another group of Cu II emission lines, which may be populated by Penning ionization involving neon metastable atoms (Ne-PI), *viz:*

$$Cu_o\ (4s\ ^2S_{1/2}) + Ne_m\ (3s\ ^3P_{0,2}) \rightarrow Cu^+* + Ne_o\ (2p^6\ ^1S_0) + e^- + \Delta E, \quad (2)$$

and also by cascade process involving transitions from higher energy levels excited by Ne-ACT.
The presence of oxygen can affect the population of neon ions and metastables and therefore changes the observed copper spectrum in neon plasma. Before discussing the effects of small quantities of oxygen on the copper line intensities in neon GD, it is essential to report the changes in sputter rate in Ne/O_2 mixtures. The normalized sputter rates of copper samples in Ne/O_2 and, for comparison, in Ne/H_2 are shown in Fig. 2. It can be seen that the presence of oxygen greatly reduces the sputter rate of copper possibly due to formation of an oxide layer on the cathode sample. To investigate the actual changes in energy level populations, it is helpful to use emission yields[27] which can be defined in eqn (3) as

$$\text{Emission yield} = \frac{\text{Intensity}}{\text{Sputter rate x conc. of analyte}} \quad (3)$$

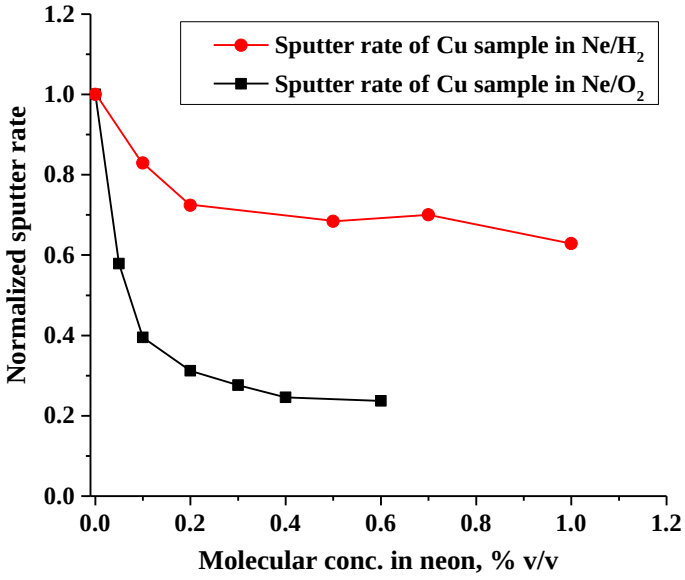

Fig. 2 Sputter rates for a copper sample in neon plasma with small amounts of molecular gases, O_2 & H_2, introduced in the discharge gas. The voltage was 700 V and the current 20 mA in all cases.

3.2 Changes in emission yields of copper ionic lines using neon/oxygen plasmas

In order to investigate the changes in emission yields of copper ionic emission lines in neon/oxygen plasma, 41 Cu II lines were studied in the spectral range 200-900 nm. A large number of copper ionic lines with excitation energies between 20-25 eV range are observable only in neon discharge. However, Cu II lines with upper energy levels above the ionization energy of neon atoms (21.564 eV) are relatively very weak as compared to lines with energy levels ~16.0-21.5 eV. In Fig. 3, to observe the overall behaviour of all the observed copper ionic lines in neon/oxygen plasma, the emission yield ratios of the Cu II lines are plotted against the total excitation energy for a low oxygen concentration (0.1% v/v) in neon. However, later in this section, the emission yield

ratios of selected Cu II lines are plotted against various oxygen concentrations. In Fig. 3, three vertical dotted red lines indicate the energy values of the two metastable states of neon (Ne_m 16.619 & 16.715 eV) and the neon ionic ground state Ne_o^+, 21.564 eV. For copper ionic lines, three groups of lines excited by various selective and non-selective excitation/ionization processes, *i.e.*, Penning ionization of copper atoms, charge transfer excitation and Penning excitation of copper ions, can be identified. More details about these selective and non-selective excitation/ionization processes in analytical glow discharges are given by Mushtaq *et al.*.[28]

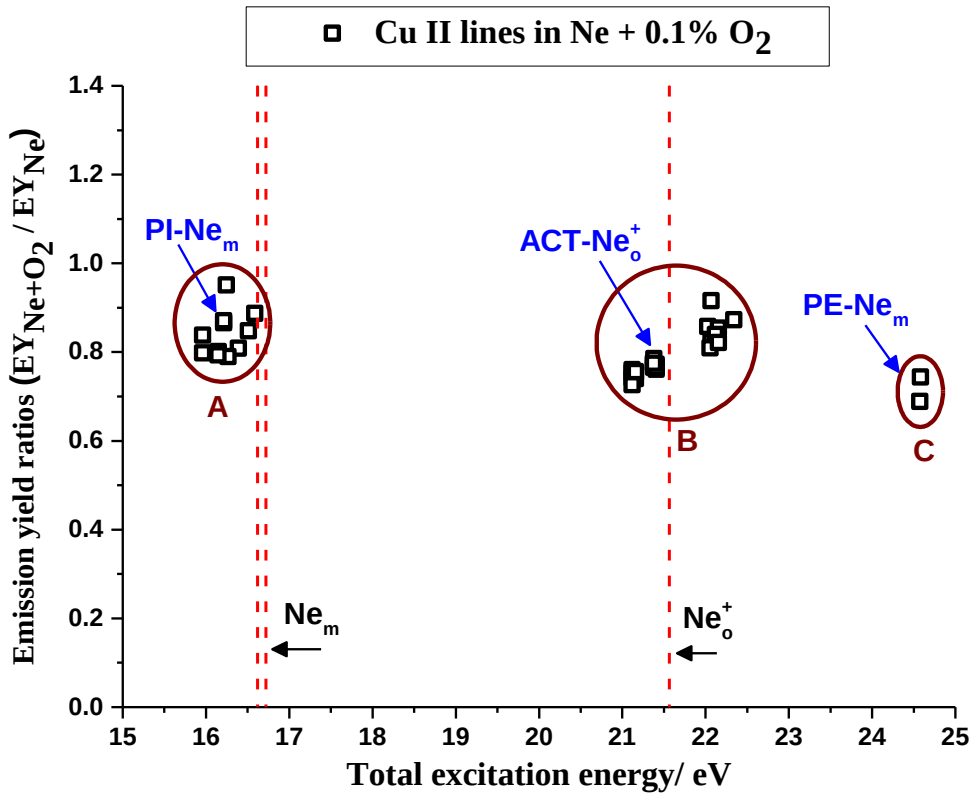

Fig. 3 Emission yield ratios for observed copper ionic lines as a function of their total excitation energies for 700 V and 20 mA for 0.1% v/v oxygen concentration in neon plasma. (PI = Penning ionization, ACT = Asymmetric charge transfer and PE = Penning excitation)

In Fig. 3 the copper ionic lines in Group A, with upper energy levels nearer to the metastable states of neon, Ne_m, are those lines which are likely to be excited by Penning ionization and also by cascade processes involving transitions from higher energy levels. On the other hand, copper ionic lines in Group B, with upper energy levels slightly below and above the ionization energy of neon are most likely excited by exoergic Ne-ACT and endoergic Ne-ACT processes involving the neon ions. 16 Cu II lines with excitation energy ~ 21.10-21.50 eV, excited by exoergic charge transfer process are the most intense of all the observed copper ionic lines. Table 4 in the appendix gives the details of these transitions.

Two copper ionic lines in Group C in Fig. 3, with upper energies about 24.581 eV, were also recorded in the Ne/Cu spectrum. These copper ionic lines are positioned about 3 eV above the ionization energy of neon atoms, and therefore not produced by Ne-ACT. The upper energy levels of these lines are about 16.855 eV above the copper ionic ground state (16.855 eV + 7.726 eV = 24.581 eV). It is possible that this group of copper ionic lines is excited by selective Penning excitation of copper ionic ground state ions, Cu_o^+,

For the Cu II 490.972 nm line:

$Cu_o^+ (3d^{10}\ ^1S_0) + Ne_m^* (3s\ ^3P_{0,2}) \rightarrow Cu^{+*} (4f\ ^3H_6) + Ne_o (2p^6\ ^1S_0) + \Delta E$ (4)

where $_o$ is a ground state, * denotes an excited state, $_m$ is a metastable state and ΔE is the kinetic energy released in the collision. This is a slightly endoergic reaction in which spin is conserved.

Some typical examples using emission yield ratios for four selected Cu II lines, 224.700, 217.941, 212.604 and 248.579 nm, from various copper ionic energy levels, against various oxygen concentrations are presented in Fig. 4. Details of these lines along with their energy values of upper and lower levels are given within Fig. 4. For the copper spectrum in pure neon plasma, the Cu II 248.579 nm line is one of the intense lines excited by neon charge transfer process. Fig. 4 shows that the emission yield ratio of this Cu II line decreases significantly with the increase of oxygen concentration in neon discharge. This indicates the reduction in neon charge transfer processes probably due to quenching of neon ions by the presence of oxygen. So far, we do not have mass spectrometry investigations on the effects of small amounts of neon discharge to show the overall changes in the total population of neon ions. However, it must be noted that mass spectrometry only indicates the total population of neon ions and cannot show changes in the population of *excited* neon ions and these may be very different from the changes in the total population of ions.

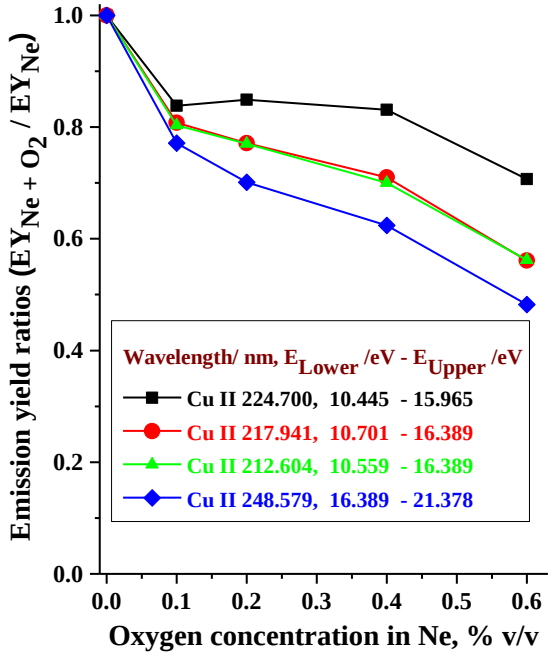

Fig. 4 Emission yield ratios for selected copper ionic lines against various oxygen concentrations in neon glow discharge for 700 V and 20 mA.

In the copper spectrum using a pure argon plasma, the Cu II 224.700 nm line is predominantly excited by charge transfer process involving argon ionic metastable state. In a pure neon plasma, due to higher critical energies of neon, this line can be excited by Penning ionization or by cascading from higher levels. However, copper lines from transitions to the upper energy level of this line have total excitation energies above the ionization of neon and therefore, the contribution from the cascade process is very small in neon discharges. In Fig. 4, it can be seen that the emission yield of this line decreases in neon/oxygen mixtures as compared to the pure neon plasma possibly due to quenching of neon metastable states. The line profiles of many neon atomic lines show changes in self reversal with the increase of oxygen in neon plasma. One typical example is shown in Fig. 5, confirming that neon metastable states are quenched in the neon/oxygen mixture possibly

as the result of energy transfer collisions with oxygen molecules, resulting in the dissociation of oxygen molecules and the direct excitation of one of the dissociative products[8], *viz:*

$$Ne_m\ (3s\ ^3P_{2,0}) + O_2\ (X\ ^3\Sigma_g^-) \rightarrow Ne_o\ (2p^6\ ^1S_0) + O\ (2p^4\ ^3P_2) + O^*\ (3p\ ^5P_{1,2,3}) \qquad (5)$$

There is a considerable decrease in the total gas pressure needed at higher oxygen concentrations in neon plasma to maintain constant voltage, see Table 1. This could also be another reason for the lower population of neon metastable states.

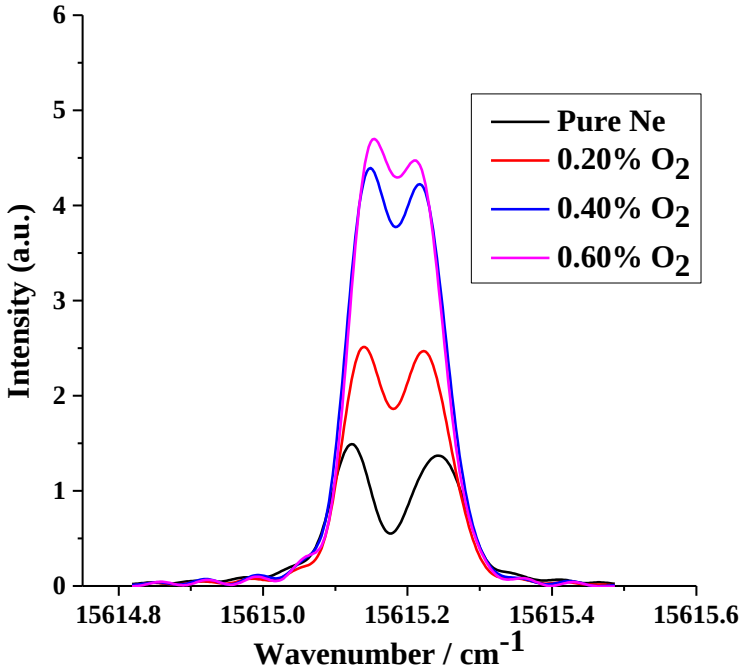

Fig. 5 Lines profiles of neon atomic 640.225 nm line, showing self-reversal for neon/oxygen plasmas. Discharge conditions were 700 V, 20 mA for a 4 mm anode tube diameter.

In Fig. 4, there are two other copper ionic lines, 217.941 & 212.604 nm, with total excitation energy nearer to the neon metastable states, which will also be excited by PI. They come from the same upper level and coincidence of their curves illustrates the accuracy of results. However, they both show a more pronounced decrease in the emission yield ratios compared to the Cu II 224.7 nm line which indicates that there is another mechanism in addition with PI process which has a major role in populating the upper energy level of these lines. By looking at the partial energy diagram of copper in Fig. 6, it can be seen that there are many Cu II lines from the higher energy levels (21-26 eV) which have transitions to the Cu II $^3F_2^o$ level at 16.389 eV, however the major contribution in populating this level comes from the Cu II 248.579 nm line which is excited by charge transfer process involving neon ions (Fig. 1a). There are three Cu II lines, 217.941, 212.604 and 208.529 nm, corresponding to transitions down to lower energy levels and depopulating the Cu II $^3F_2^o$ level. The presence of oxygen reduces Ne-ACT and hence the population of the Cu II $^3F_2^o$ level by radiative decay from higher energy levels. Therefore, the 217.941 nm and 212.604 nm lines show an emission yield decrease midway between that of the 248.579 nm and 224.7 nm lines with added oxygen.

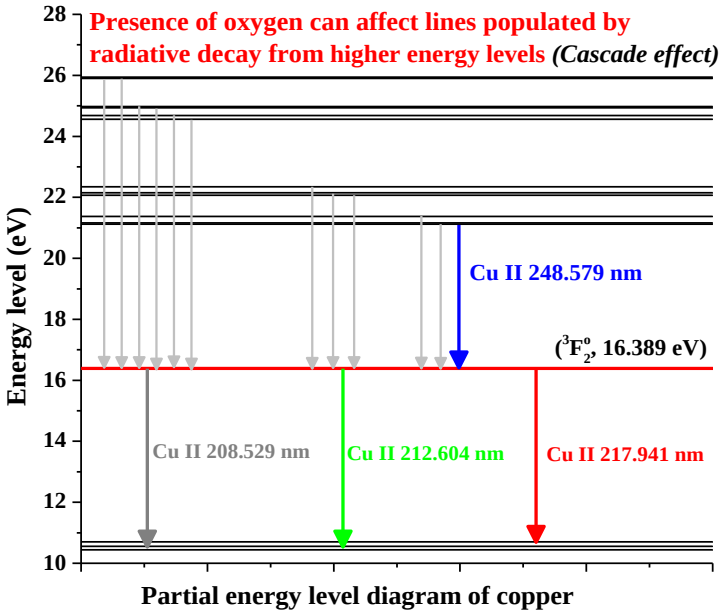

Fig. 6 Partial Cu II energy level diagram, showing various transitions from higher energy levels populating the upper energy level ($^3F_2^o$, 16.389 eV) of the three Cu II lines (217.941, 212.604 and 208.529 nm). The colours correspond to those used in Fig. 4.

So far, it is observed that the presence of oxygen can affect existing excitation processes (Ne-ACT & Ne-PI) by the plasma gas. However, the presence of oxygen can also itself cause selective excitation in analytical glow discharges. For the selective excitation process, there must be ionic states of sputtered atoms with appropriate energy to be excited, however, in the case of copper as cathode material, there are no suitable copper ionic energy levels (near to 13.6 eV, the ionization energy of oxygen atom) which can be selectively excited by oxygen. On the other hand, in the case of iron as cathode material, it was shown in our previous paper[10] that there are several iron ionic energy levels close to the ionization energy of oxygen, which are suitable for both the exoergic O-ACT and endoergic O-ACT. It was also reported that many Fe II lines which are not only excited by charge transfer process involving oxygen ions in their ground state but also by oxygen ionic metastable levels ($2p^3\ ^2D$, 16.934 eV), which have lifetimes of several hours.[10]

3.3 Changes in emission yields of copper atomic lines using neon/oxygen plasmas

The changes in emission yield ratios of the 40 copper atomic lines observed in this study against their excitation energy are shown in Fig. 7 for two different oxygen concentrations. It can be seen that at low oxygen concentrations the changes in emission yield ratios are not distinct, however, it is important to note that the changes (enhancement due to change in self-absorption & three body collisional recombination or reduction where neutralization process is suppressed) in emission yield ratios for Cu I lines are more pronounced at higher oxygen concentrations in neon. In Fig. 7(b), the Cu I 324.754 nm line is the strong resonance line and therefore subject to self-absorption. As it is noticed in Fig. 2, that the sputter rate changes significantly in the presence of oxygen, therefore, changes in emission yield are greater for Cu I 324.754 nm line. A significant increase in emission yield ratios for copper atomic lines with excitation energy near to 5 eV is also observed in presence of 0.6% v/v oxygen in neon. This enhancement of copper atomic lines in the presence of oxygen is likely to be due to a three body collision, leading to the formation of oxygen molecules. This effect is not apparent when lower oxygen concentrations in neon plasma are used. More details for this effect are discussed in another paper.[29] The copper atomic lines with total excitation energies about 6.0-7.5 eV, show significant decrease in the emission yield ratios in neon/oxygen mixtures. In pure neon plasma, these copper atomic lines are probably excited by electronic excitation (EE) and also

by neutralization of copper ions. However, in the presence of oxygen in neon, the emission yield ratios of copper atomic lines are decreased significantly possibly due to a decrease in the total population of copper ions.

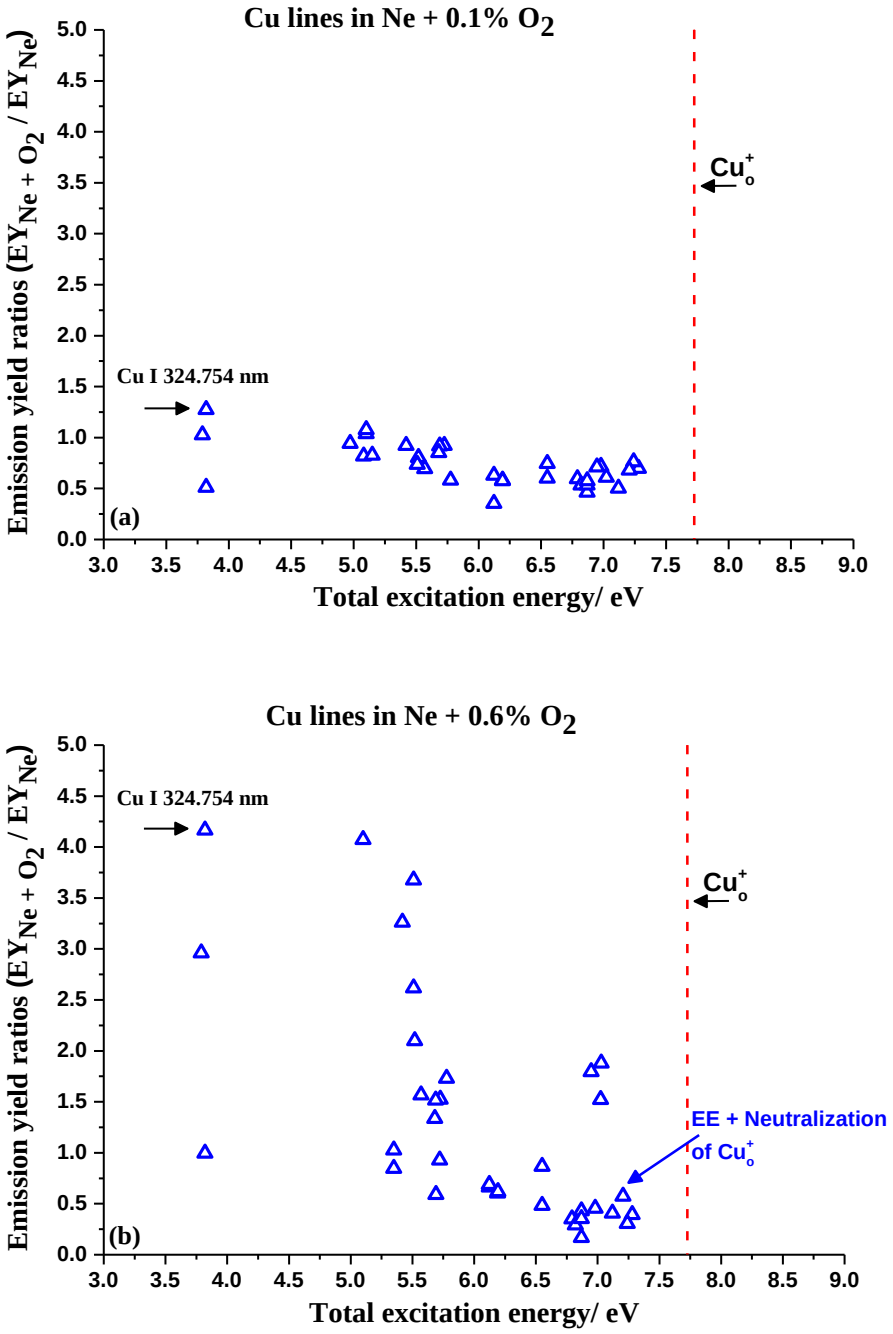

Fig. 7 Emission yield ratios for observed copper atomic lines as a function of their total excitation energy for 700 V and 20 mA for (a) 0.1 and (b) 0.6% v/v oxygen concentrations in neon plasma. (EE = electronic excitation)

The emission yield ratios for selected copper atomic lines against various oxygen concentrations in neon GD are shown in Fig. 8. Both Cu I 324.754 and 327.396 nm lines are resonance lines and decay to the copper atom ground state, and therefore, subject to self-absorption. With the addition of oxygen in neon plasma, the sputter rate of copper decreases significantly resulting in a decrease in copper atom density. Hence, there is change in self-absorption of these resonance lines with the addition of oxygen. These copper atomic lines are from close lying upper energies having similar

populations; in the case of the 324.754 nm line, the statistical weight of the upper level is 4 while that of the upper level of the 327.396 nm line is 2, therefore, the absorption co-efficient of the former is twice that of later. Hence in the presence of oxygen, the 324.754 nm line shows a greater change in emission yield as compared to the 327.396 nm line. The contribution of self-absorption to the changes in the emission yield is highlighted by the plot for the 510.554 nm line which is a transition from the same upper level as the Cu I 324.754 nm line but terminates at the 1.390 eV metastable level and has a much lower transition probability[30] and is therefore subject to little, if any, self-absorption, *i.e.*, in Fig. 8 the plot for 510.554 nm reveals the true changes in the population of upper energy level.

The Cu I 327.982 nm line also shows a very significant increase in the emission yield ratios at higher oxygen concentrations. Up to 0.2% v/v concentration, the ratio is more or less unchanged, however, at higher oxygen concentrations this line shows pronounced increase in emission yields due to the above mentioned three body collisional recombination of oxygen atoms. The emission yield ratios of other copper atomic lines, e.g. 515.324 and 406.264 nm, decrease in the presence of oxygen possibly due to a significant contribution to the population of their upper levels from neutralization of copper ionic levels; the ion number density probably decreases significantly in the presence of oxygen.

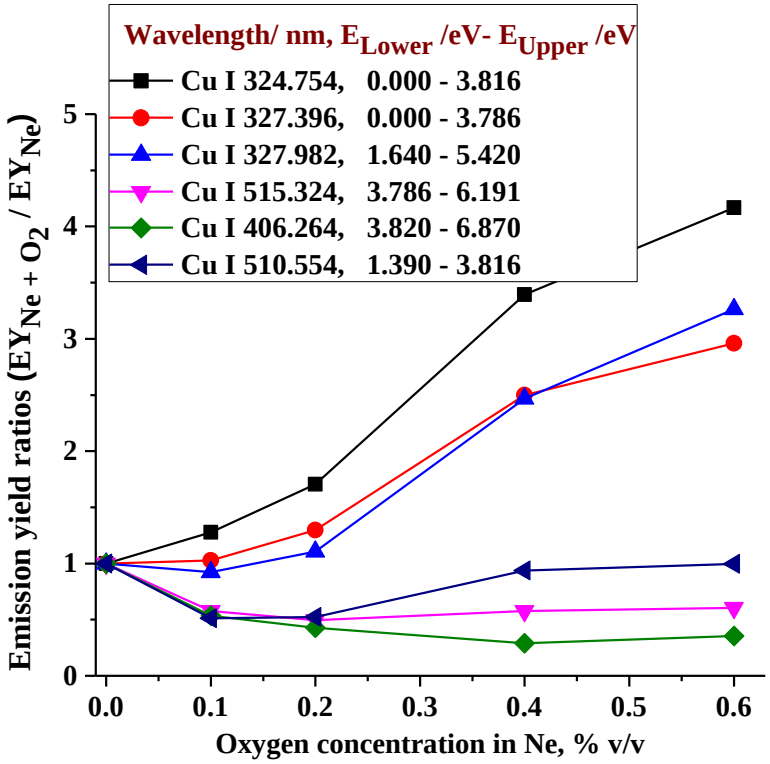

Fig. 8 Emission yield ratios for selected copper atomic lines against various oxygen concentrations in neon glow discharge for 700 V and 20 mA.

3.4 Changes in intensity ratios of neon ionic lines using neon/oxygen plasmas

Changes in sputter rates are irrelevant in the case of neon atomic and ionic lines and therefore intensity ratios are used for neon in this study rather than emission yield ratios. However, it must be remembered that to maintain constant voltage and constant current with added oxygen, a significant reduction in the gas pressure is required (see Table 1) and this will affect the intensities of neon lines in two ways, by changing the number density of neon atoms and by altering the electron energy distribution. Fig. 9 shows the intensity ratios of various neon ionic lines plotted against their

total excitation energies at 0.6% v/v oxygen concentration in a neon plasma. Details of the transitions for observed neon lines are given in Table 5 in the appendix. Differing behaviours in the emission intensities of neon ionic lines occur in the presence of oxygen. The majority of the neon ionic lines show a decrease in their intensity ratios on addition of oxygen. In Fig. 9, a trend of cascading for neon ionic lines with excitation energies of about ~56 eV and ~53 eV can be observed. In the figure the lower levels of the transitions in Group D are the upper levels of the lines in Group A. Consequently, the decrease of the intensities of the lines in Group D reduces the cascading contribution to the upper states of lines in Group A and so causes a fall in their intensities.

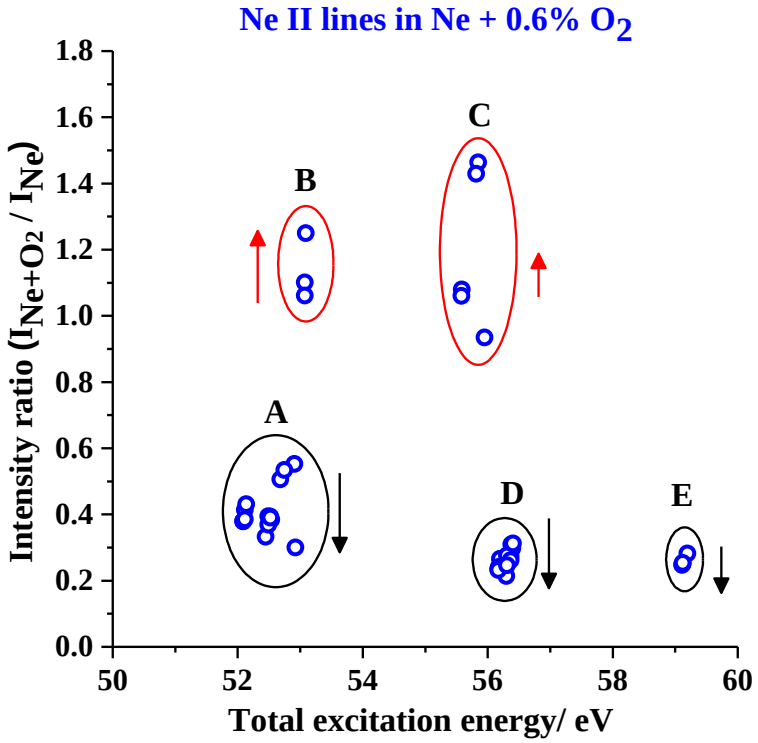

Fig. 9 Intensity ratios for observed neon ionic lines plotted against total excitation energy of upper levels for 0.6% v/v oxygen concentration for 700 V and 20 mA.

Similarly, the intensities of the Ne II lines in Group C increase slightly with the addition of oxygen, and hence the intensities of the Ne II lines in Group B also increase. The effect of oxygen on the cascade process is more pronounced in the case of neon/oxygen than argon/oxygen mixtures.[31]

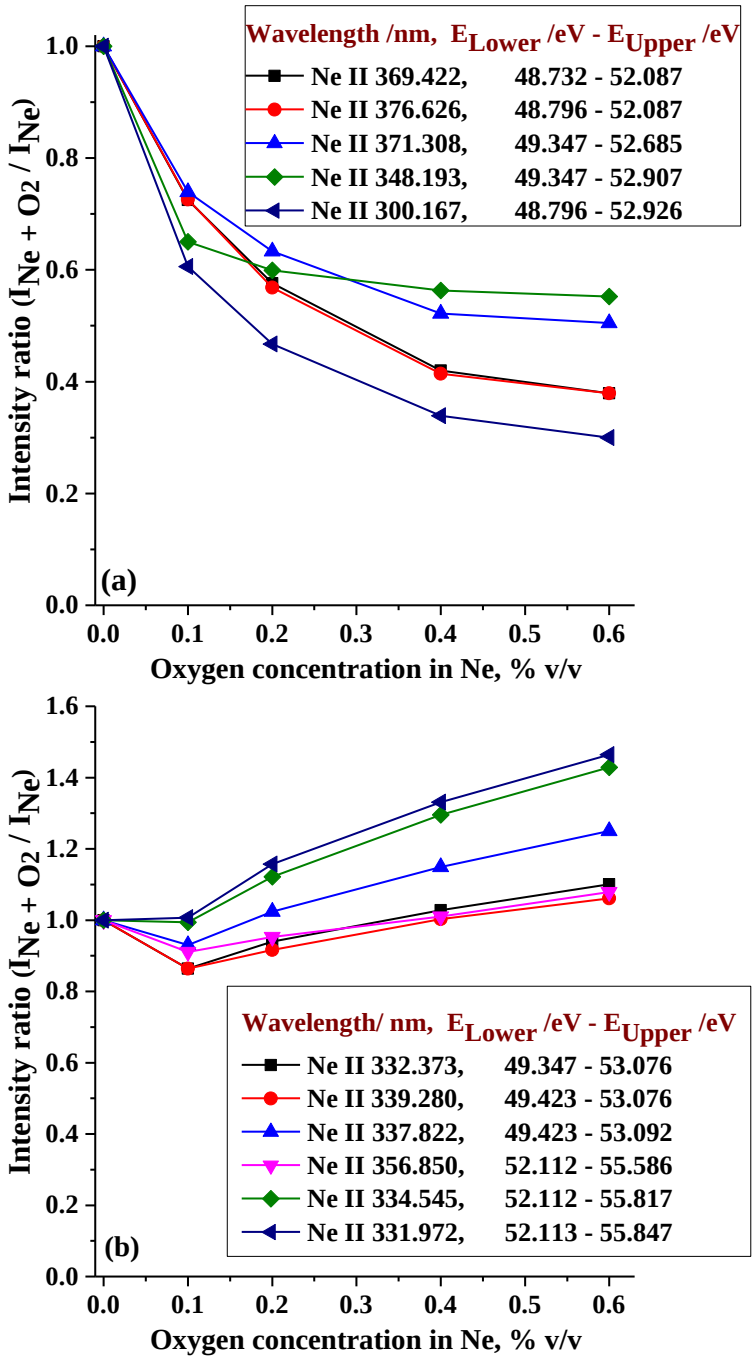

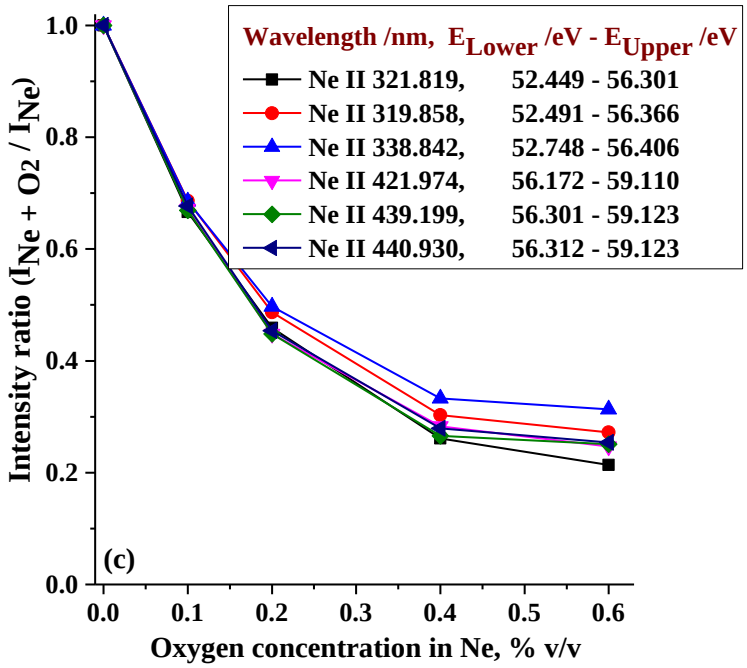

Fig. 10 Intensity ratios for neon ionic lines plotted against various oxygen concentrations in neon glow discharge for 700 V and 20 mA. a) lines from Group A in Fig. 9, b) lines from Groups B & C, c) lines from Groups D & E.

The intensity ratios for selected neon ionic lines from different excitation energy ranges are plotted against various oxygen concentrations in neon GD in Fig. 10. The neon ionic lines presented in Fig. 10(a) are taken from Group A and all show a smooth decrease in the intensity ratios with the increase of oxygen concentrations. In Fig. 10(b), three neon ionic lines are from Group B and other three are from Group C. These neon ionic lines show a different behaviour than the other Ne II lines. On the other hand, the Ne II lines presented in Fig. 10(c) are from Group D and E, and also show a significant decrease in their intensity ratios with the progressive increase of oxygen in neon plasma. It is likely that neon ionic lines are excited directly from the ground state of neon atoms by electron impact excitation.[13] The presence of oxygen in neon GD may affect the excitation process for neon ionic lines by altering the number density and the energy distribution of the electrons. The decrease in electron temperature produced by higher electron thermalisation rates due to vibrational and rotational excitation of oxygen molecules in neon/oxygen mixtures can account for the significant drop in the intensity of neon ionic lines, as few high energy electrons are available.

3.5 Changes in intensity ratios of neon atomic lines using neon/oxygen plasmas

In Fig. 11(a), the intensity ratios of 45 neon atomic lines are plotted against their excitation energy for 0.6% v/v oxygen concentration in a neon plasma. It can be seen that the intensities of the majority of the neon atomic lines from the $2s^2 2p^5 3s$ configuration (energy ca.18-19 eV) have increased by varying amounts although a few decrease. On the other hand, Ne I lines corresponding to transitions from higher energy levels (20.0-20.5 eV) show decreases in their intensities when oxygen is present. A similar general trend to the change in emission intensities of Ar I lines is observed in argon/oxygen mixtures[6]; the emission intensities of the majority of the Ar I lines from the $3s^2 3p^5 4p$ energy levels increase and lines from higher energy levels decrease.

The main processes populating the upper levels of the observed Ne I lines are shown in the partial energy level diagram in Fig. 11(b). The upper levels of the neon lines, as presented in Fig. 11(a), lie in the square box, and can be differentiated into two energy groups (18-19 eV) and (20.0-20.5 eV). They can be populated either by direct electronic excitation from the ground state of the neon atom

or by a two step excitation involving the neon metastable states. The higher upper energy levels of neon atomic lines can also be populated by the neutralization of neon ions. The presence of oxygen in neon plasma by altering the number density of electrons, neon metastables or neon ions can affect significantly these excitation processes.

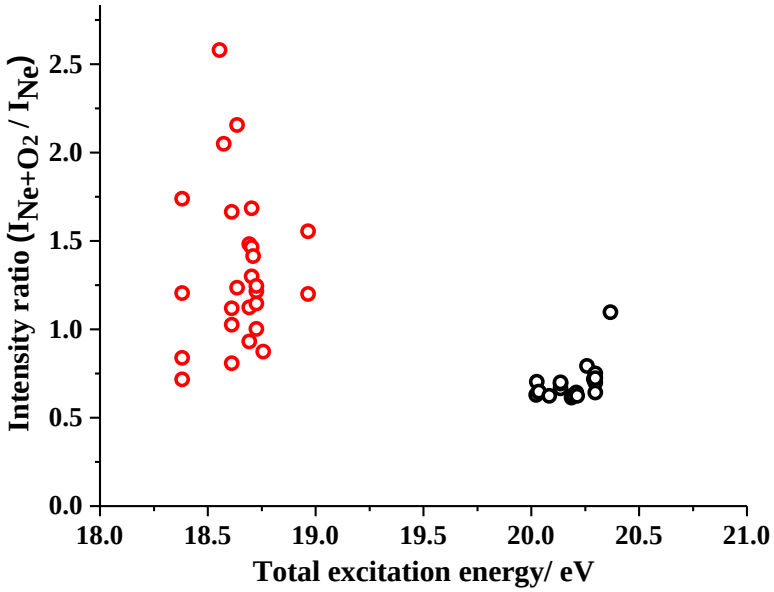

(a) Intensity ratios of Ne I lines

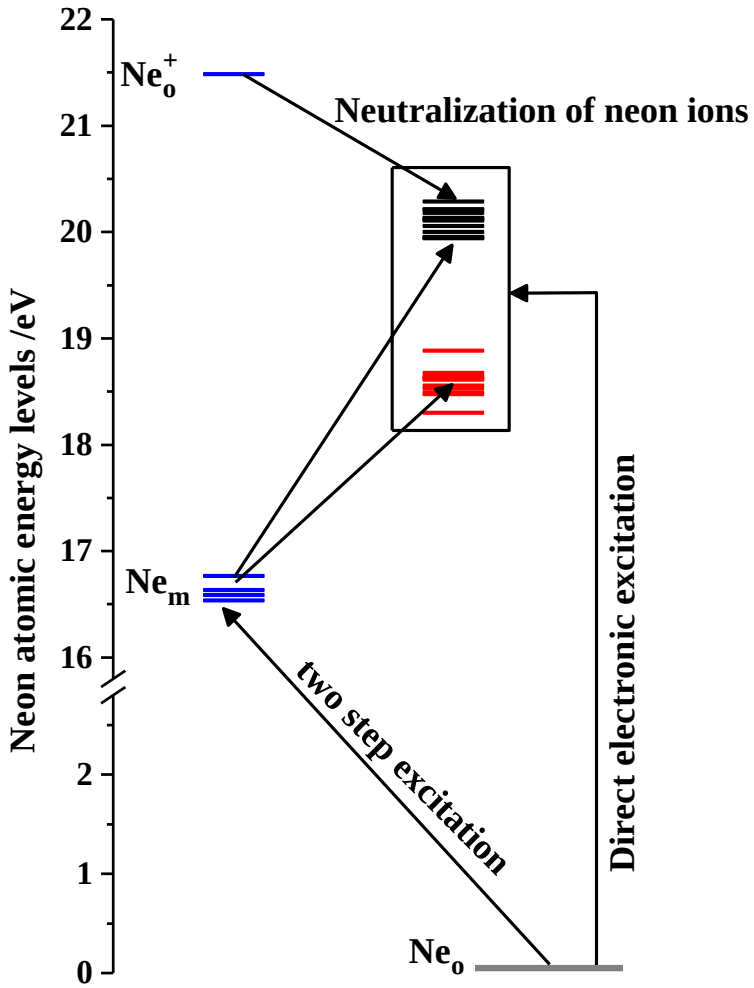

(b) Excitation mechanisms of neon atomic levels

Fig. 11 (a) Intensity ratios for observed neon atomic lines are plotted against total excitation energies for 0.6% v/v oxygen concentration in neon glow discharge (700 V, 20 mA). (b) Excitation mechanisms of neon atomic levels. The upper levels for lines, the intensity ratios of which are included in Fig. 11a, lie within the rectangular box.

Emission line intensity ratios of selected neon atomic lines from Fig. 11(a), with various upper energies are shown as functions of the oxygen concentration in Fig. 12(a-c). Details of the transitions for these Ne I lines are given within the figures. It can be seen that all the selected Ne I lines in Fig. 12(a) & (b) have transitions to the metastable levels or nearby quasi-metastable levels.[30] The non-linear increase in emission intensities of neon atomic lines in Fig. 12(a) with the progressive increase of oxygen is most probably due to the change in the number density of neon metastable states, resulting in a decrease in self-absorption (see Fig. 5.). Thus, although the 703.241 nm and 724.517 nm line come from the same upper level, the 703.241 nm line, which has a higher transition probability (Table 3) and is therefore more affected by self absorption, shows the higher intensity increase when oxygen is added. Šmíd (private communication) has shown that under similar discharge conditions, when hydrogen is added to argon, the measured line widths of the majority of the analogous Ar I lines (from the $3s^2 3p^5 4p$ configuration) decrease, indicating reduced self absorption, while the width of lines from higher levels with much lower transition probabilities remain unchanged – *i.e.* the lines are not affected by self absorption. Šmíd also showed a similar effect on the measured widths of Ne I lines when nitrogen is added to a neon discharge.

The neon atomic lines from the higher upper energy levels shown in black in Fig. 12(b) exhibit significant decreases in their emission intensity with the increase of oxygen concentration. The

excitation of the neon atomic lines from higher energy levels can be due to direct electronic excitation, a two step excitation involving the neon metastable levels and or the neutralization of neon ions by slow electrons. The quenching of these neon atomic lines could be the result of the quenching by oxygen of both neon metastable states and neon ions. There is likely to be little self-absorption affecting these lines, with the possible exception of the 352.047 nm line, which has an abnormally high transition probability for this group of transitions.

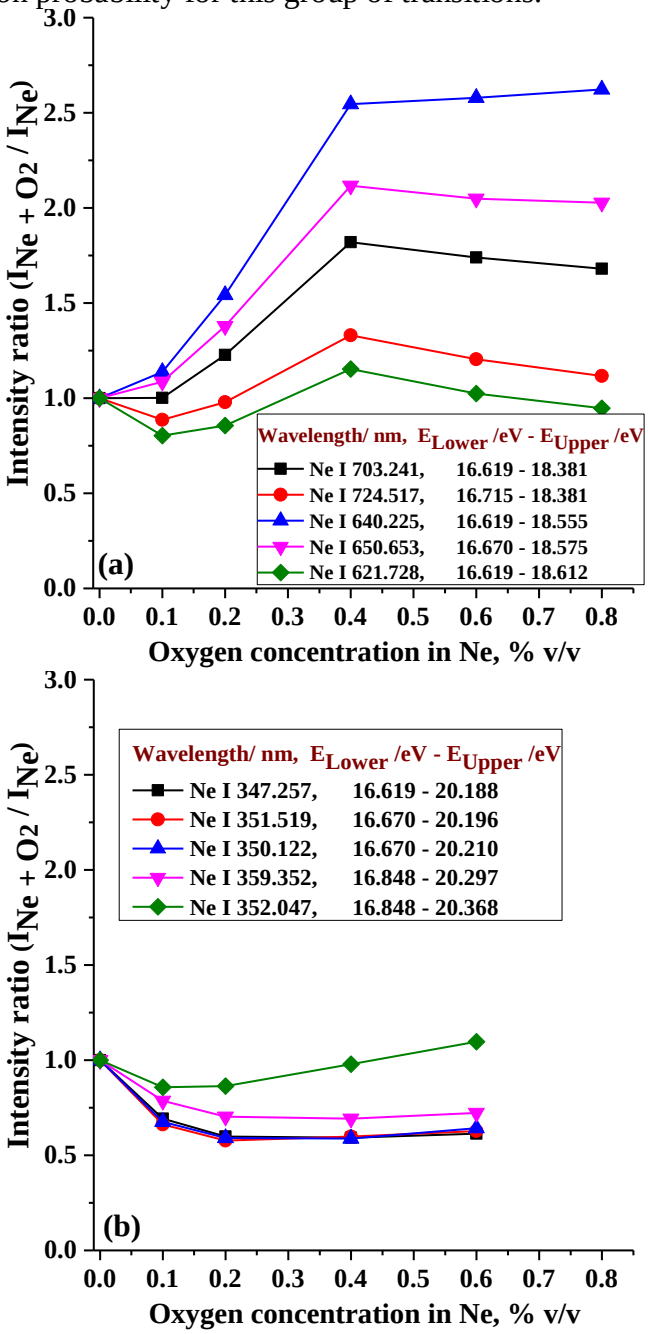

Fig. 12 Intensity ratios for selected neon atomic lines against various oxygen concentrations in neon glow discharge for 700 V and 20 mA. The higher oxygen concentration used for the neon lines at longer wavelengths confirms the changing trend of the line intensities.

4. Conclusions

The results of a comprehensive multi-line study on the effect of small quantities of oxygen in a neon glow discharge with a copper sample are reported and discussed. The ratios of emission yields of copper with and without added oxygen are used in this study as the presence of oxygen in neon greatly reduces the sputter rate of copper samples. The higher energy of the neon metastable states and the higher ionization energy compared to argon have a major effect on the appearance of the spectrum. The presence of small quantities of oxygen in the GD affects the populations of neon metastable levels and ions and so changes the observed spectrum.

In a neon GD, sample lines with upper levels with total excitation energy ~ 21.5 eV are populated by asymmetric charge transfer. Those with total excitation energy ~ 16.7 eV are not only populated by Penning ionization, but also by radiative transitions from higher levels. Emission yields of copper ionic lines excited by Ne-ACT fall considerably when oxygen is added, probably due to a fall in the Ne^+ population; the presence of oxygen can also significantly affect Cu II levels populated by radiative decay from higher energy levels. Lines predominantly excited by PI, for example 224.7 nm, exhibit a smaller fall than ACT-excited lines with oxygen addition. Copper ionic lines populated by PI and also by radiative decay from higher energy levels show a decrease midway between those Cu II lines excited by PI and Ne-ACT with added oxygen. For copper atomic lines, it is observed that at low oxygen concentrations it is not possible to distinguish the causes of the changes in emission yield ratios; however, at higher oxygen concentrations the changes in the ratios (such as enhancement due to changes in self-absorption & three body collisional recombination of oxygen atoms or reduction where a drop in the Cu II ion population suppresses the neutralization process) become more pronounced. It must be noted that oxygen concentrations used in our experiments are considerably higher than those expected from analytical samples[32]; however, at such higher concentrations various effects can be more clearly seen and interpreted.

For neon ionic lines, cascading with excitation energies about ~56 eV and ~53 eV could be observed. It is apparent that with the addition of oxygen to the neon plasma, the intensities of Ne II lines having upper energy levels within the total excitation energy range ~56 eV drop and consequently the intensities of the Ne II lines from lower energy levels within the total excitation energy range ~53 eV also drop. In the case of neon atomic lines, a similar general trend to the change in emission intensities for Ar I lines in argon/oxygen mixtures as reported previously[6] is observed; the emission intensities of the majority of the Ne I lines from lower energy levels increase and lines from higher energy levels decrease. The increase in emission intensities of Ne I lines with the progressive increase of oxygen is most probably due to a fall in the number density of neon metastable states, resulting in decreased self-absorption. On the other hand, the smooth decrease in Ne I lines from higher energy levels could be due to quenching in neon/oxygen mixtures of the neon metastable atoms and neon ions, which contribute to exciting these levels by either two step excitation or neutralization of neon ions. Glow discharge mass spectrometry experiments for neon/oxygen mixtures are planned to obtain detailed results for the changes in total populations of neon ions with added oxygen. It is hoped that these experiments will provide firm evidence to support our GD-OES results.

Acknowledgements

The authors thank Drs Volker Hoffmann, Denis Klemm and Varvara Efimova for experimental support in measurements at IFW Dresden of sample crater volumes used in this work. SM acknowledges the support for his ESR post under the EC funded Research Training Network GLADNET, EC contract MRTN-CT-2006-035459 during his experimental work.

References

1. W. Fischer, W. Naoumidis and H. Nickel, "Effects of a controlled addition of nitrogen and oxygen to argon on the analytical parameters of glow discharge optical emission spectrometry" *J. Anal. At. Spectrom.,* 1994, **9**, 375-380.
2. K. Wagatsuma and K. Hirokawa, "Effect of oxygen addition to an argon glow-discharge plasma source in atomic emission spectrometry", *Anal. Chim. Acta,* 1995, **306**, 193-200.
3. B. Fernández, N. Bordel, C. Pérez, R. Pereiro and A. Sanz-Medel, "The influence of hydrogen, nitrogen or oxygen additions to radiofrequency argon glow discharges for optical emission spectrometry" *J. Anal. At. Spectrom.*, 2002, **17**, 1549-1555.
4. B. Fernández, N. Bordel, R. Pereiro and A. Sanz-Medel, "Investigations of the effect of hydrogen, nitrogen or oxygen on the in-depth profile analysis by radiofrequency argon glow discharge-optical emission spectrometry" *J. Anal. At. Spectrom.,* 2003, **18**, 151-156.
5. A. Bogaerts, "Effects of oxygen addition to argon glow discharge: A hybrid Monte Carlo-fluid modeling investigation" *Spectrochim. Acta Part B*, 2009, **64**, 1266-1279.
6. S. Mushtaq, E. B.M. Steers, J. C. Pickering, T. Gusarova, P. Šmíd and V. Weinstein, "Effects of traces of oxygen on Grimm-type glow discharges in argon" *J. Anal. At. Spectrom.,* 2011, **26**, 766-775.
7. S. Mushtaq, J. C. Pickering, E. B.M. Steers, P. Horvath, J. A. Whitby and J. Micher, "The role of oxygen in analytical glow discharges: GD-OES and GD-ToF-MS studies" *J. Anal. At. Spectrom.,* 2011, **26**, 1746-1755.
8. W. R. Bennett, Jr. W. L. Faust, R. A. McFarlane and C. K.N. Patel, "Dissociative excitation transfer and optical mass oscillation" *Phys. Rev. Lett.,* 1962, **8**, 470-474.
9. C. R. Aita and M. E. Marhic, "Optical emission from neon/oxygen rf sputtering glow discharges" *J. Vac. Sci. Technol. A,* 1983, **1**, 69-73.
10. S. Mushtaq, E. B.M. Steers, J. C. Pickering and V. Weinstein, "Asymmetric charge transfer involving the ions of added gases (oxygen or hydrogen) in Grimm-type glow discharges in argon or neon" *J. Anal. Spectrom.,* 2012, **27**, 1264-1273.
11. G. Nave, S. Johansson, R. C. M. Learner, A. P. Thorne and J. W. Brault, A new multiplet table for Fe I, *ApJS*, 1994, **94**, 221-459.
12. O. S. Duffendack and J. G. Black, Studies on the spectra of Cu I, Cu II and Mn II by means of a vacuum tungsten furnace, *Phys. Rev.*,1929, **34**, 35-43.
13. F. J. De Hoog, J. R. McNeil, and G. J. Collins, and K. B. Persson, Discharge studies of the Ne-Cu laser, Jour. Appl. Phys., 1977, **48(9)**, 3701-3704.
14. R. Solanki, E. L. Latush, D. C. Gerstenberger, W. M. Fairbank, Jr., and G. J. Collins, Hollow-cathode excitation of ion laser transitions in noble-gas mixtures, *Appl. Phys. Lett.*, 1979, **35(4)**, 317-319.
15. K. R. Hess and W. W. Harrison, The role of metastable atoms in glow discharge ionization processes, Anal. Chem., 1988, **60(7)**, 691-696.
16. A. Bogaerts and R. Gijbels, Comparison of argon and neon as discharge gases in a direct-current glow discharge, *Spectrochim. Acta Part B*, 1997, **52**, 553-565.
17. E. B.M. Steers, and A. P. Thorne, Application of high-resolution Fourier transform spectrometry to the study of glow discharge sources Part I. Excitation of iron and chromium

spectra in a microwave boosted glow discharge source, *J. Anal. At. Spectrom.*, 1993, **8**, 309-315.

18. F. Leis and E. B.M. Steers, Some properties of a microwave boosted glow discharge source using neon as the operating gas, *Fresenius J. Anal. Chem.*, 1996, **355,** 873-875.

19. Z. Weiss, *Glow* discharge excitation and matrix effects in the Zn-Al-Cu system in argon and neon, *Spectrochim. Acta Part B*, 2007, **62**, 787.

20. K. Wagatsuma and K. Hirokawa, Observations of Bismuth and Lead ionic emission lines excited from Grimm-type glow discharge plasmas with pure neon and neon-argon mixtures, *J. Anal. At. Spectrom.*, 1989, **4**, 525-528.

21. K. Wagatsuma and K. Hirokawa, Spectrometric studies of excitation mechanisms on singly-ionized copper emission lines in Grimm-type glow discharge plasmas with helium mixture technique, *Spectrochim. Acta Part B,* 1991, **46**, 269-281.

22. K. Wagatsuma, K. Hirokawa, and N. Yamashita, Detection of fluorine emission lines from Grimm-type glow discharge plasmas – use of neon as the plasma gas, *Anal. Chim. Acta,* 1996, **324**, 147-154.

23. V-D Hodoroaba, E. B.M. Steers, V. Hoffmann and K. Wetzig, "The effect of small quantities of hydrogen on a glow discharge in neon. Comparison with the argon case" *J. Anal. At. Spectrom.*, 2001, **16**, 43-49.

24. V. Weinstein, Ph.D. Thesis, London Metropolitan University, 2011.

25. J. C. Pickering, "High resolution Fourier transform spectroscopy with the Imperial College (IC) UV-FT spectrometer, and its applications to astrophysics and atmospheric physics: a review" *Vib. Spectrosc.*, 2002, **29**, 27-43.

26. E. B.M. Steers and R. J. Fielding, "Charge-transfer excitation processes in the Grimm lamp" *J. Anal. At. Spectrom.*, 1987, **2**, 239-244.

27. Z. Weiss, "Emission yields and the standard model in glow discharge optical emission spectroscopy: Links to the underlying physics and analytical interpretation of the experimental data", *Spectrochim. Acta, Part B,* 2006, **61**, 121-133.

28. S. Mushtaq, E. B.M. Steers, J. C. Pickering and K. Putyera, "Selective and non-selective excitation/ionization processes in analytical glow discharge: excitation of the ionic spectra in argon/helium mixed plasmas" *J. Anal. At. Spectrom.*, 2014, **29**, 681-695.

29. S. Mushtaq, E. B.M. Steers, J. C. Pickering and P. Šmíd, "Enhancement of analyte atomic lines with excitation energies of about 5 eV in the presence of molecular gases in analytical glow discharges" *J. Anal. At. Spectrom.*, submitted June, 2014.

30. NIST Atomic Spectra Data base: www.physics.nist.gov/PhysRefData/ASD, May 2014.

31. S. Mushtaq, Ph.D. thesis, Imperial College, London, 2011.

32. S. Mushtaq, V. Hoffmann, E. B.M. Steers and J. C. Pickering, "Comparison of a sample containing oxide with a pure sample with argon-oxygen mixtures" *J. Anal. At. Spectrom.*, 2012, **27**, 1423-1431.

33. A. R. Striganov and N. S. Sventitskij, *Table of Spectral Lines of Neutral and Ionized Atoms,* Plenum Data Corporation, New York, 1968.

34. J. Sugar and A. Musgrove, *J. Phys. Chem. Ref. Data*, 1990, **19(3)**, 527-616.

Table 1: Variations of the gas pressure during the experiments in Ne/O_2 with copper sample at constant dc electrical parameters (20 mA and 700 V) in GD.

Neon/oxygen	
O_2 Concentration (% v/v), ± 5 %	**Pressure (Torr) ± 0.02**
0	12.0
0.04	11.1
0.10	10.8
0.20	9.50
0.40	8.66
0.60	8.26
0.80	8.16

Table 2 Details of experimental measurements

Experiment	Spectral region	Wavelength range/nm	Photomultiplier tube dectector	Filter	Resolution/ cm^{-1}
Cu-Ne/O_2	"UV"	200-300	R166	-	0.040
Cu-Ne/O_2	"Visible"	295-590	IP28	WG295	0.040
Cu-Ne/O_2	"Near infrared"	450-900	R928	LP47	0.033

Table 3 The selected Ne I emission lines as presented in the Fig. 12 with details of the transitions (from Ref. 30) and approximate relative intensities as recorded in this work.

λ/nm	I_{line}*	Lower energy/ eV	Upper Energy/ eV	Configurations		Terms	J_i-J_k**	A*** (10^7 s^{-1})
				Lower	Upper			
Ne I 703.241	VS	16.619	18.381	$2p^5(^2P^o_{3/2})3s$	$2p^5(^2P^o_{3/2})3p$	$^2[3/2]^o$-$^2[1/2]$	2-1	2.53
Ne I 724.517	S	16.670	18.381	$2p^5(^2P^o_{3/2})3s$	$2p^5(^2P^o_{3/2})3p$	$^2[3/2]^o$-$^2[1/2]$	1-1	0.93
Ne I 640.225	VS	16.619	18.555	$2p^5(^2P^o_{3/2})3s$	$2p^5(^2P^o_{3/2})3p$	$^2[3/2]^o$-$^2[5/2]$	2-3	5.14
Ne I 650.653	VS	16.670	18.575	$2p^5(^2P^o_{3/2})3s$	$2p^5(^2P^o_{3/2})3p$	$^2[3/2]^o$-$^2[5/2]$	1-2	3.00
Ne I 621.728	S	16.619	18.612	$2p^5(^2P^o_{3/2})3s$	$2p^5(^2P^o_{3/2})3p$	$^2[3/2]^o$-$^2[3/2]$	2-1	0.64
Ne I 347.257	M	16.619	20.188	$2p^5(^2P^o_{3/2})3s$	$2p^5(^2P^o_{3/2})4p$	$^2[3/2]^o$-$^2[5/2]$	2-3	0.17
Ne I 351.519	W	16.670	20.196	$2p^5(^2P^o_{3/2})3s$	$2p^5(^2P^o_{3/2})4p$	$^2[3/2]^o$-$^2[5/2]$	1-2	0.06
Ne I 350.122	M	16.670	20.210	$2p^5(^2P^o_{3/2})3s$	$2p^5(^2P^o_{3/2})4p$	$^2[3/2]^o$-$^2[3/2]$	1-1	0.12
Ne I 359.352	M	16.848	20.297	$2p^5(^2P^o_{1/2})3s$	$2p^5(^2P^o_{1/2})4p$	$^2[1/2]^o$-$^2[3/2]$	1-2	0.09
Ne I 352.047	S	16.848	20.368	$2p^5(^2P^o_{1/2})3s$	$2p^5(^2P^o_{1/2})4p$	$^2[1/2]^o$-$^2[1/2]$	1-0	0.93

* ***I* is the observed line intensity in pure neon plasma; VS= very strong; S= strong; M= medium and W= weak.**

** ***k* is for upper state and *i* is for lower state**

*** ***A* is the transition probability**

Appendix

Table 4 The observed copper emission lines discussed in this work with details of the transitions (from ref. 33, 34) and relative intensities as recorded in this work.

Wavelength/ nm	I_{Ar}*	Lower energy/ eV	Upper energy/ eV	Lower configurations	Upper configurations	Terms	J_i-J_k**
Cu I 327.396	VS	0.000	3.786	$3d^{10}4s$	$3d^{10}4p$	^2S-$^2P^o$	1/2 - 1/2
Cu I 578.213	W	1.642	3.786	$3d^9(^2D)4s^2$	$3d^{10}4p$	^2D-$^2P^o$	3/2 - 1/2
Cu I 324.754	VS	0.000	3.816	$3d^{10}4s$	$3d^{10}4p$	^2S-$^2P^o$	1/2 - 3/2
Cu I 510.554	S	1.389	3.816	$3d^9(^2D)4s^2$	$3d^{10}4p$	^2D-$^2P^o$	5/2 - 3/2
Cu I 249.215	W	0.000	4.973	$3d^{10}4s$	$3d^9(^2D)4s4p(^3P)$	^2S-$^4P^o$	1/2 - 3/2
Cu I 244.163	VW	0.000	5.076	$3d^{10}4s$	$3d^9(^2D)4s4p(^3P)$	^2S-$^4P^o$	1/2 - 1/2
Cu I 333.784	M	1.389	5.102	$3d^9(^2D)4s^2$	$3d^9(^2D)4s4p(^3P)$	^2D-$^4F^o$	5/2 - 7/2
Cu I 353.038	W	1.642	5.153	$3d^9(^2D)4s^2$	$3d^9(^2D)4s4p(^3P)$	^2D-$^4F^o$	3/2 - 5/2
Cu I 793.311	W	3.785	5.348	$3d^{10}4p$	$3d^{10}5s$	$^2P^o$-^2S	1/2 - 1/2
Cu I 809.264	M	3.816	5.348	$3d^{10}4p$	$3d^{10}5s$	$^2P^o$-^2S	3/2 - 1/2
Cu I 307.380	VW	1.389	5.421	$3d^9(^2D)4s^2$	$3d^9(^2D)4s4p(^3P)$	^2D-$^2F^o$	5/2 - 5/2
Cu I 327.982	M	1.642	5.421	$3d^9(^2D)4s^2$	$3d^9(^2D)4s4p(^3P)$	^2D-$^2F^o$	3/2 - 5/2
Cu I 301.084	W	1.389	5.505	$3d^9(^2D)4s^2$	$3d^9(^2D)4s4p(^3P)$	^2D-$^4D^o$	5/2 - 5/2
Cu I 320.823	W	1.642	5.505	$3d^9(^2D)4s^2$	$3d^9(^2D)4s4p(^3P)$	^2D-$^4D^o$	3/2 - 5/2
Cu I 319.410	W	1.642	5.522	$3d^9(^2D)4s^2$	$3d^9(^2D)4s4p(^3P)$	^2D-$^4D^o$	3/2 - 3/2
Cu I 222.570	W	0.000	5.568	$3d^{10}4s$	$3d^9(^2D)4s4p(^3P)$	^2S-$^4D^o$	1/2 - 1/2
Cu I 218.172	W	0.000	5.681	$3d^{10}4s$	$3d^9(^2D)4s4p(^3P)$	^2S-$^2P^o$	1/2 - 1/2
Cu I 217.895	VW	0.000	5.688	$3d^{10}4s$	$3d^9(^2D)4s4p(^3P)$	^2S-$^2P^o$	1/2 - 3/2
Cu I 306.341	W	1.642	5.688	$3d^9(^2D)4s^2$	$3d^9(^2D)4s4p(^3P)$	^2D-$^2P^o$	3/2 - 3/2
Cu I 303.610	W	1.642	5.724	$3d^9(^2D)4s^2$	$3d^9(^2D)4s4p(^3P)$	^2D-$^2D^o$	3/2 - 3/2
Cu I 216.510	W	0.000	5.724	$3d^{10}4s$	$3d^9(^2D)4s4p(^3P)$	^2S-$^2D^o$	1/2 - 3/2
Cu I 282.437	VW	1.389	5.777	$3d^9(^2D)4s^2$	$3d^9(^2D)4s4p(^3P)$	^2D-$^2D^o$	5/2 - 5/2
Cu I 261.837	W	1.389	6.122	$3d^9(^2D)4s^2$	$3d^{10}5p$	^2D-$^2P^o$	5/2 - 3/2
Cu I 276.637	VW	1.642	6.122	$3d^9(^2D)4s^2$	$3d^{10}5p$	^2D-$^2P^o$	3/2 - 3/2
Cu I 515.324	S	3.785	6.191	$3d^{10}4p$	$3d^{10}4d$	$^2P^o$-^2D	1/2 - 3/2
Cu I 521.820	VS	3.816	6.192	$3d^{10}4p$	$3d^{10}4d$	$^2P^o$-^2D	3/2 - 5/2
Cu I 448.035	W	3.785	6.552	$3d^{10}4p$	$3d^{10}6s$	$^2P^o$-^2S	1/2 - 1/2
Cu I 453.078	M	3.816	6.552	$3d^{10}4p$	$3d^{10}6s$	$^2P^o$-^2S	3/2 - 1/2
Cu I 229.384	S	1.389	6.792	$3d^9(^2D)4s^2$	$3d^{10}6p$	^2D-$^2P^o$	5/2 - 3/2
Cu I 239.263	VW	1.642	6.822	$3d^9(^2D)4s^2$	$3d^{10}6p$	^2D-$^2P^o$	3/2 - 1/2
Cu I 402.263	M	3.785	6.867	$3d^{10}4p$	$3d^{10}5d$	$^2P^o$-^2D	1/2 - 3/2
Cu I 406.323	W	3.816	6.867	$3d^{10}4p$	$3d^{10}5d$	$^2P^o$-^2D	3/2 - 3/2
Cu I 223.008	M	1.389	6.946	$3d^9(^2D)4s^2$	$3d^9(^2D)4s4p(^1P)$	^2D-$^2F^o$	5/2 - 7/2
Cu I 221.459	M	1.389	6.985	$3d^9(^2D)4s^2$	$3d^9(^2D)4s4p(^1P)$	^2D-$^2P^o$	5/2 - 3/2
Cu I 219.959	M	1.389	7.023	$3d^9(^2D)4s^2$	$3d^9(^2D)4s4p(^1P)$	^2D-$^2D^o$	5/2 - 5/2
Cu I 386.174	VW	3.816	7.026	$3d^{10}4p$	$3d^{10}7s$	$^2P^o$-^2S	3/2 - 1/2
Cu I 226.309	VW	1.642	7.119	$3d^9(^2D)4s^2$	$3d^{10}7p$	^2D-$^2P^o$	3/2 - 1/2
Cu I 222.778	M	1.642	7.205	$3d^9(^2D)4s^2$	$3d^9(^2D)4s4p(^1P)$	^2D-$^2F^o$	3/2 – 5/2
Cu I 221.566	W	1.642	7.236	$3d^9(^2D)4s^2$	$3d^9(^2D)4s4p(^1P)$	^2D-$^2P^o$	3/2 – 1/2
Cu I 219.976	M	1.642	7.276	$3d^9(^2D)4s^2$	$3d^9(^2D)4s4p(^1P)$	^2D-$^2D^o$	3/2 – 3/2
Cu_o^+			**7.7264**		**$3d^{10}$**	**^1S_o**	
Cu II 224.700	S	10.445	15.961	$3d^9(^2D)4s$	$3d^9(^2D)4p$	^3D – $^3P^o$	3 – 2
Cu II 229.437	W	10.559	15.961	$3d^9(^2D)4s$	$3d^9(^2D)4p$	^3D – $^3P^o$	2 – 2
Cu II 248.965	VW	10.982	15.961	$3d^9(^2D)4s$	$3d^9(^2D)4p$	^1D – $^3P^o$	2 – 2
Cu II 227.626	M	10.701	16.147	$3d^9(^2D)4s$	$3d^9(^2D)4p$	^3D – $^3P^o$	1 – 1

Cu II 221.811	M	10.559	16.147	$3d^9(^2D)4s$	$3d^9(^2D)4p$	$^3D - ^3P^o$	2 – 1
Cu II 236.989	W	10.982	16.212	$3d^9(^2D)4s$	$3d^9(^2D)4p$	$^1D - ^3F^o$	2 – 3
Cu II 219.227	M	10.559	16.212	$3d^9(^2D)4s$	$3d^9(^2D)4p$	$^1D - ^3F^o$	2 – 3
Cu II 213.598	M	10.445	16.248	$3d^9(^2D)4s$	$3d^9(^2D)4p$	$^3D - ^3F^o$	3 – 4
Cu II 222.886	M	10.701	16.262	$3d^9(^2D)4s$	$3d^9(^2D)4p$	$^3D - ^3P^o$	1 – 0
Cu II 217.941	M	10.701	16.389	$3d^9(^2D)4s$	$3d^9(^2D)4p$	$^3D - ^3F^o$	1 – 2
Cu II 212.604	M	10.559	16.389	$3d^9(^2D)4s$	$3d^9(^2D)4p$	$^3D - ^3F^o$	2 – 2
Cu II 224.262	M	10.982	16.509	$3d^9(^2D)4s$	$3d^9(^2D)4p$	$^1D - ^3D^o$	2 – 3
Cu II 221.027	M	10.982	16.590	$3d^9(^2D)4s$	$3d^9(^2D)4p$	$^1D - ^3D^o$	2 – 2
Cu II 240.334	M	15.961	21.118	$3d^9(^2D)4p$	$3d^9(^2D)5s$	$^3P^o - ^3D$	2 – 3
Cu II 252.659	W	16.212	21.118	$3d^9(^2D)4p$	$3d^9(^2D)5s$	$^3F^o - ^3D$	3 – 3
Cu II 254.480	S	16.248	21.118	$3d^9(^2D)4p$	$3d^9(^2D)5s$	$^3F^o - ^3D$	4 – 3
Cu II 268.930	M	16.509	21.118	$3d^9(^2D)4p$	$3d^9(^2D)5s$	$^3D^o - ^3D$	3 – 3
Cu II 276.967	W	16.643	21.118	$3d^9(^2D)4p$	$3d^9(^2D)5s$	$^3D^o - ^3D$	3 – 3
Cu II 247.333	M	16.147	21.158	$3d^9(^2D)4p$	$3d^9(^2D)5s$	$^3P^o - ^3D$	1 – 2
Cu II 250.627	S	16.212	21.158	$3d^9(^2D)4p$	$3d^9(^2D)5s$	$^3F^o - ^3D$	3 – 2
Cu II 271.351	S	16.590	21.158	$3d^9(^2D)4p$	$3d^9(^2D)5s$	$^3D^o - ^3D$	2 – 2
Cu II 242.443	S	16.262	21.375	$3d^9(^2D)4p$	$3d^9(^2D)5s$	$^3P^o - ^3D$	0 – 1
Cu II 248.579	VVS	16.389	21.375	$3d^9(^2D)4p$	$3d^9(^2D)5s$	$^3F^o - ^3D$	2 – 1
Cu II 270.318	S	16.789	21.375	$3d^9(^2D)4p$	$3d^9(^2D)5s$	$^3D^o - ^3D$	1 – 1
Cu II 259.053	S	16.389	21.375	$3d^9(^2D)4p$	$3d^9(^2D)5s$	$^3D^o - ^3D$	2 – 1
Cu II 272.167	S	16.821	21.375	$3d^9(^2D)4p$	$3d^9(^2D)5s$	$^1D^o - ^3D$	2 – 1
Cu II 271.877	S	16.851	21.410	$3d^9(^2D)4p$	$3d^9(^2D)5s$	$^1P^o - ^1D$	1 – 2
Cu II 246.850	M	16.389	21.410	$3d^9(^2D)4p$	$3d^9(^2D)5s$	$^3F^o - ^1D$	2 – 2
Cu II 252.930	VS	16.509	21.410	$3d^9(^2D)4p$	$3d^9(^2D)5s$	$^3D^o - ^1D$	3 – 2
Cu II 260.027	S	16.647	21.410	$3d^9(^2D)4p$	$3d^9(^2D)5s$	$^3D^o - ^1D$	3 – 2
Cu II 270.096	S	16.821	21.410	$3d^9(^2D)4p$	$3d^9(^2D)5s$	$^1D^o - ^1D$	2 – 2
Cu II 213.434	W	16.248	22.055	$3d^9(^2D)4p$	$3d^9(^2D)4d$	$^3F^o - ^3G$	4 – 5
Cu II 211.731	W	16.212	22.066	$3d^9(^2D)4p$	$3d^9(^2D)4d$	$^3F^o - ^3G$	3 – 4
Cu II 237.63	VW	16.851	22.067	$3d^9(^2D)4p$	$3d^9(^2D)4d$	$^1P^o - ^3P$	1 – 1
Cu II 220.980	W	16.509	22.118	$3d^9(^2D)4p$	$3d^9(^2D)4d$	$^3D^o - ^3D$	3 – 3
Cu II 222.985	M	16.590	22.149	$3d^9(^2D)4p$	$3d^9(^2D)4d$	$^3D^o - ^3F$	2 – 3
Cu II 219.568	M	16.509	22.149	$3d^9(^2D)4p$	$3d^9(^2D)4d$	$^3D^o - ^3F$	3 – 3
Cu II 222.678	W	16.590	22.156	$3d^9(^2D)4p$	$3d^9(^2D)4d$	$^3D^o - ^3D$	2 – 2
Cu II 217.498	M	16.643	22.342	$3d^9(^2D)4p$	$3d^9(^2D)4d$	$^3D^o - ^1G$	3 – 4
Cu II 468.199	W	21.924	24.571	$3d^9(^2D)4d$	$3d^9(^2D_{5/2})4f$	$^3S - ^3P^o$	1 – 1
Cu II 490.973	W	22.055	24.579	$3d^9(^2D)4d$	$3d^9(^2D_{5/2})4f$	$^3G - ^3H^o$	5 – 6

Note: all the value of the excitation energy of ionic lines given are the total excitation energy from the ground state of the atom (*i.e.* excitation energy + ionization energy).

*** *I* is the observed line intensity in pure neon plasma; VS= very strong; S= strong; M= medium; W= weak and VW= very weak.**

**** *k* is for upper state and *i* is for lower state.**

Table 5 The observed neon emission lines discussed in this work with details of the transitions (from Ref. 30) and approximate relative intensities as recorded in this work.

Wavelength/ Nm	I_{Ar}*	Lower energy/ eV	Upper energy/ eV	Lower configurations	Upper configurations	Terms	J_i-J_k**
Ne I 703.241	VS	16.619	18.381	$2s^22p^5(^2P^o_{3/2})3s$	$2s^22p^5(^2P^o_{3/2})3p$	$^2[3/2]^o$ - $^2[1/2]$	2 - 1
Ne I 724.517	VS	16.670	18.381	$2s^22p^5(^2P^o_{3/2})3s$	$2s^22p^5(^2P^o_{3/2})3p$	$^2[3/2]^o$ - $^2[1/2]$	1 – 1
Ne I 743.889	S	16.715	18.381	$2s^22p^5(^2P^o_{1/2})3s$	$2s^22p^5(^2P^o_{3/2})3p$	$^2[1/2]^o$ - $^2[1/2]$	0 – 1
Ne I 808.246	W	16.848	18.381	$2s^22p^5(^2P^o_{1/2})3s$	$2s^22p^5(^2P^o_{3/2})3p$	$^2[1/2]^o$ - $^2[1/2]$	1 – 1
Ne I 640.225	VS	16.619	18.555	$2s^22p^5(^2P^o_{3/2})3s$	$2s^22p^5(^2P^o_{3/2})3p$	$^2[3/2]^o$ - $^2[5/2]$	2 – 3
Ne I 650.653	VS	16.670	18.575	$2s^22p^5(^2P^o_{3/2})3s$	$2s^22p^5(^2P^o_{3/2})3p$	$^2[3/2]^o$ - $^2[5/2]$	1 – 2
Ne I 717.394	S	16.848	18.575	$2s^22p^5(^2P^o_{1/2})3s$	$2s^22p^5(^2P^o_{3/2})3p$	$^2[1/2]^o$ - $^2[5/2]$	1 – 2
Ne I 621.728	VS	16.619	18.612	$2s^22p^5(^2P^o_{3/2})3s$	$2s^22p^5(^2P^o_{3/2})3p$	$^2[3/2]^o$ - $^2[3/2]$	2 – 1
Ne I 638.300	S	16.670	18.612	$2s^22p^5(^2P^o_{3/2})3s$	$2s^22p^5(^2P^o_{3/2})3p$	$^2[3/2]^o$ - $^2[3/2]$	1 – 1
Ne I 653.288	VS	16.715	18.612	$2s^22p^5(^2P^o_{1/2})3s$	$2s^22p^5(^2P^o_{3/2})3p$	$^2[1/2]^o$ - $^2[3/2]$	0 – 1
Ne I 702.406	S	16.848	18.612	$2s^22p^5(^2P^o_{1/2})3s$	$2s^22p^5(^2P^o_{3/2})3p$	$^2[1/2]^o$ - $^2[3/2]$	1 – 1
Ne I 614.306	VS	16.619	18.636	$2s^22p^5(^2P^o_{3/2})3s$	$2s^22p^5(^2P^o_{3/2})3p$	$^2[3/2]^o$ - $^2[3/2]$	2 – 2
Ne I 692.946	VS	16.848	18.636	$2s^22p^5(^2P^o_{1/2})3s$	$2s^22p^5(^2P^o_{3/2})3p$	$^2[1/2]^o$ - $^2[3/2]$	1 – 2
Ne I 597.553	S	16.619	18.693	$2s^22p^5(^2P^o_{3/2})3s$	$2s^22p^5(^2P^o_{1/2})3p$	$^2[3/2]^o$ - $^2[3/2]$	2 – 1
Ne I 626.650	VS	16.715	18.693	$2s^22p^5(^2P^o_{1/2})3s$	$2s^22p^5(^2P^o_{1/2})3p$	$^2[1/2]^o$ - $^2[3/2]$	0 – 1
Ne I 671.704	VS	16.848	18.693	$2s^22p^5(^2P^o_{1/2})3s$	$2s^22p^5(^2P^o_{1/2})3p$	$^2[1/2]^o$ - $^2[3/2]$	1 – 1
Ne I 594.484	VS	16.619	18.704	$2s^22p^5(^2P^o_{3/2})3s$	$2s^22p^5(^2P^o_{1/2})3p$	$^2[3/2]^o$ - $^2[3/2]$	2 – 2
Ne I 609.616	VS	16.670	18.704	$2s^22p^5(^2P^o_{3/2})3s$	$2s^22p^5(^2P^o_{1/2})3p$	$^2[3/2]^o$ - $^2[3/2]$	1 – 2
Ne I 667.828	VS	16.848	18.704	$2s^22p^5(^2P^o_{1/2})3s$	$2s^22p^5(^2P^o_{1/2})3p$	$^2[1/2]^o$ - $^2[3/2]$	1 – 2
Ne I 607.434	VS	16.670	18.711	$2s^22p^5(^2P^o_{3/2})3s$	$2s^22p^5(^2P^o_{3/2})3p$	$^2[3/2]^o$ - $^2[1/2]$	1 – 0
Ne I 588.190	VS	16.619	18.726	$2s^22p^5(^2P^o_{3/2})3s$	$2s^22p^5(^2P^o_{1/2})3p$	$^2[3/2]^o$ - $^2[1/2]$	2 – 1
Ne I 603.000	VS	16.670	18.726	$2s^22p^5(^2P^o_{3/2})3s$	$2s^22p^5(^2P^o_{1/2})3p$	$^2[3/2]^o$ - $^2[1/2]$	1 – 1
Ne I 616.360	VS	16.715	18.726	$2s^22p^5(^2P^o_{1/2})3s$	$2s^22p^5(^2P^o_{1/2})3p$	$^2[1/2]^o$ - $^2[1/2]$	0 – 1
Ne I 659.896	VS	16.848	18.726	$2s^22p^5(^2P^o_{1/2})3s$	$2s^22p^5(^2P^o_{1/2})3p$	$^2[1/2]^o$ - $^2[1/2]$	1 – 1
Ne I 540.056	S	16.670	18.965	$2s^22p^5(^2P^o_{3/2})3s$	$2s^22p^5(^2P^o_{1/2})3p$	$^2[3/2]^o$ - $^2[1/2]$	1 – 0
Ne I 585.249	VS	16.848	18.965	$2s^22p^5(^2P^o_{1/2})3s$	$2s^22p^5(^2P^o_{1/2})3p$	$^2[1/2]^o$ - $^2[1/2]$	1 – 0
Ne I 754.405	M	18.381	20.024	$2s^22p^5(^2P^o_{3/2})3p$	$2s^22p^5(^2P^o_{3/2})3d$	$^2[1/2]$ - $^2[1/2]^o$	1 – 0
Ne I 753.578	M	18.381	20.026	$2s^22p^5(^2P^o_{3/2})3p$	$2s^22p^5(^2P^o_{3/2})3d$	$^2[1/2]$ - $^2[1/2]^o$	1 – 1
Ne I 837.761	M	18.555	20.034	$2s^22p^5(^2P^o_{3/2})3p$	$2s^22p^5(^2P^o_{3/2})3d$	$^2[5/2]$ - $^2[7/2]^o$	3 – 4
Ne I 748.888	M	18.381	20.036	$2s^22p^5(^2P^o_{3/2})3p$	$2s^22p^5(^2P^o_{3/2})3d$	$^2[1/2]$ - $^2[3/2]^o$	1 – 2
Ne I 830.032	M	18.555	20.048	$2s^22p^5(^2P^o_{3/2})3p$	$2s^22p^5(^2P^o_{3/2})3d$	$^2[5/2]$ - $^2[5/2]^o$	3 – 3
Ne I 794.318	M	18.575	20.136	$2s^22p^5(^2P^o_{3/2})3p$	$2s^22p^5(^2P^o_{1/2})3d$	$^2[5/2]$ - $^2[5/2]^o$	2 – 3
Ne I 813.641	M	18.612	20.136	$2s^22p^5(^2P^o_{3/2})3p$	$2s^22p^5(^2P^o_{1/2})3d$	$^2[3/2]$ - $^2[5/2]^o$	1 – 2
Ne I 705.911	M	18.381	20.137	$2s^22p^5(^2P^o_{3/2})3p$	$2s^22p^5(^2P^o_{1/2})3d$	$^2[1/2]$ - $^2[3/2]^o$	1 – 2
Ne I 347.257	M	16.619	20.188	$2s^22p^5(^2P^o_{3/2})3s$	$2s^22p^5(^2P^o_{3/2})4p$	$^2[3/2]^o$ - $^2[5/2]$	2 – 3
Ne I 351.519	M	16.670	20.196	$2s^22p^5(^2P^o_{3/2})3s$	$2s^22p^5(^2P^o_{3/2})4p$	$^2[3/2]^o$ - $^2[5/2]$	1 – 2
Ne I 346.433	W	16.619	20.197	$2s^22p^5(^2P^o_{3/2})3s$	$2s^22p^5(^2P^o_{3/2})4p$	$^2[3/2]^o$ - $^2[5/2]$	2 – 2
Ne I 350.122	M	16.670	20.210	$2s^22p^5(^2P^o_{3/2})3s$	$2s^22p^5(^2P^o_{3/2})4p$	$^2[3/2]^o$ - $^2[3/2]$	1 – 1
Ne I 344.770	M	16.619	20.214	$2s^22p^5(^2P^o_{3/2})3s$	$2s^22p^5(^2P^o_{3/2})4p$	$^2[3/2]^o$ - $^2[3/2]$	2 – 2
Ne I 345.419	W	16.670	20.259	$2s^22p^5(^2P^o_{3/2})3s$	$2s^22p^5(^2P^o_{3/2})4p$	$^2[3/2]^o$ - $^2[1/2]$	1 – 0
Ne I 346.657	M	16.715	20.290	$2s^22p^5(^2P^o_{1/2})3s$	$2s^22p^5(^2P^o_{1/2})4p$	$^2[1/2]^o$ - $^2[3/2]$	0 – 1
Ne I 336.990	W	16.619	20.297	$2s^22p^5(^2P^o_{3/2})3s$	$2s^22p^5(^2P^o_{1/2})4p$	$^2[3/2]^o$ - $^2[1/2]$	2 – 1
Ne I 341.790	W	16.670	20.297	$2s^22p^5(^2P^o_{3/2})3s$	$2s^22p^5(^2P^o_{1/2})4p$	$^2[3/2]^o$ - $^2[3/2]$	1 – 2
Ne I 359.352	M	16.848	20.297	$2s^22p^5(^2P^o_{1/2})3s$	$2s^22p^5(^2P^o_{1/2})4p$	$^2[1/2]^o$ - $^2[3/2]$	1 – 2
Ne I 352.047	S	16.848	20.368	$2s^22p^5(^2P^o_{1/2})3s$	$2s^22p^5(^2P^o_{1/2})4p$	$^2[1/2]^o$ - $^2[1/2]$	1 – 0
Ne_o^+			**21.564**		**$2s^2\ 2p^5$**	**$^2P^o$**	**3/2**

Ne II lines in Group A presented in Fig. 9							
Ne II 369.422	S	48.732	52.087	$2s^22p^4(^3P)3s$	$2s^22p^4(^3P)3p$	$^4P - ^4P^o$	5/2 – 5/2
Ne II 376.626	M	48.796	52.087	$2s^22p^4(^3P)3s$	$2s^22p^4(^3P)3p$	$^4P - ^4P^o$	3/2 – 5/2
Ne II 366.407	S	48.732	52.115	$2s^22p^4(^3P)3s$	$2s^22p^4(^3P)3p$	$^4P - ^4P^o$	5/2 – 3/2
Ne II 377.714	M	48.834	52.115	$2s^22p^4(^3P)3s$	$2s^22p^4(^3P)3p$	$^4P - ^4P^o$	1/2 – 3/2
Ne II 370.962	M	48.796	52.138	$2s^22p^4(^3P)3s$	$2s^22p^4(^3P)3p$	$^4P - ^4P^o$	3/2 – 1/2
Ne II 333.483	VS	48.732	52.449	$2s^22p^4(^3P)3s$	$2s^22p^4(^3P)3p$	$^4P - ^4D^o$	5/2 – 7/2
Ne II 329.772	M	48.732	52.491	$2s^22p^4(^3P)3s$	$2s^22p^4(^3P)3p$	$^4P - ^4D^o$	5/2 – 5/2
Ne II 335.502	S	48.796	52.491	$2s^22p^4(^3P)3s$	$2s^22p^4(^3P)3p$	$^4P - ^4D^o$	3/2 – 5/2
Ne II 332.715	S	48.796	52.522	$2s^22p^4(^3P)3s$	$2s^22p^4(^3P)3p$	$^4P - ^4D^o$	3/2 – 3/2
Ne II 336.059	M	48.834	52.522	$2s^22p^4(^3P)3s$	$2s^22p^4(^3P)3p$	$^4P - ^4D^o$	1/2 – 3/2
Ne II 334.439	M	48.834	52.540	$2s^22p^4(^3P)3s$	$2s^22p^4(^3P)3p$	$^4P - ^4D^o$	1/2 – 1/2
Ne II 371.308	S	49.347	52.685	$2s^22p^4(^3P)3s$	$2s^22p^4(^3P)3p$	$^2P - ^4D^o$	3/2 – 5/2
Ne II 372.710	M	49.423	52.748	$2s^22p^4(^3P)3s$	$2s^22p^4(^3P)3p$	$^2P - ^2D^o$	1/2 – 3/2
Ne II 348.193	M	49.347	52.907	$2s^22p^4(^3P)3s$	$2s^22p^4(^3P)3p$	$^2P - ^2S^o$	3/2 – 1/2
Ne II 300.167	M	48.796	52.926	$2s^22p^4(^3P)3s$	$2s^22p^4(^3P)3p$	$^4P - ^4S^o$	3/2 – 3/2
Ne II lines in Group B & C presented in Fig. 9							
Ne II 332.373	VS	49.347	53.076	$2s^22p^4(^3P)3s$	$2s^22p^4(^3P)3p$	$^2P - ^2P^o$	3/2 – 3/2
Ne II 339.280	M	49.423	53.076	$2s^22p^4(^3P)3s$	$2s^22p^4(^3P)3p$	$^2P - ^2P^o$	1/2 – 3/2
Ne II 337.822	S	49.423	53.076	$2s^22p^4(^3P)3s$	$2s^22p^4(^3P)3p$	$^2P - ^2P^o$	1/2 – 1/2
Ne II 357.461	M	52.113	55.580	$2s^22p^4(^1D)3s$	$2s^22p^4(^1D)3p$	$^2D - ^2F^o$	3/2 – 5/2
Ne II 356.850	S	52.113	55.586	$2s^22p^4(^1D)3s$	$2s^22p^4(^1D)3p$	$^2D - ^2F^o$	5/2 – 7/2
Ne II 334.545	S	52.112	55.817	$2s^22p^4(^1D)3s$	$2s^22p^4(^1D)3p$	$^2D - ^2P^o$	5/2 – 3/2
Ne II 331.972	S	52.113	55.847	$2s^22p^4(^1D)3s$	$2s^22p^4(^1D)3p$	$^2D - ^2P^o$	3/2 – 1/2
Ne II 323.007	M	52.112	55.950	$2s^22p^4(^1D)3s$	$2s^22p^4(^1D)3p$	$^2D - ^2D^o$	5/2 – 5/2
Ne II lines in Group D presented in Fig. 9							
Ne II 303.446	M	52.087	56.172	$2s^22p^4(^3P)3p$	$2s^22p^4(^3P)3d$	$^4P^o - ^4D$	5/2 – 7/2
Ne II 332.916	M	52.449	56.172	$2s^22p^4(^3P)3p$	$2s^22p^4(^3P)3d$	$^4D^o - ^4D$	7/2 – 7/2
Ne II 302.701	M	52.088	56.182	$2s^22p^4(^3P)3p$	$2s^22p^4(^3P)3d$	$^4P^o - ^4D$	5/2 – 5/2
Ne II 304.755	M	52.115	56.182	$2s^22p^4(^3P)3p$	$2s^22p^4(^3P)3d$	$^4P^o - ^4D$	3/2 – 5/2
Ne II 303.771	W	52.115	56.195	$2s^22p^4(^3P)3p$	$2s^22p^4(^3P)3d$	$^4P^o - ^4D$	3/2 – 3/2
Ne II 321.819	S	52.449	56.301	$2s^22p^4(^3P)3p$	$2s^22p^4(^3P)3d$	$^4D^o - ^4F$	7/2 – 9/2
Ne II 324.409	M	52.491	56.312	$2s^22p^4(^3P)3p$	$2s^22p^4(^3P)3d$	$^4D^o - ^2F$	5/2 – 7/2
Ne II 341.768	M	52.685	56.312	$2s^22p^4(^3P)3p$	$2s^22p^4(^3P)3d$	$^2D^o - ^2F$	5/2 – 7/2
Ne II 319.858	M	52.491	56.366	$2s^22p^4(^3P)3p$	$2s^22p^4(^3P)3d$	$^4D^o - ^4F$	5/2 – 7/2
Ne II 336.721	M	52.685	56.366	$2s^22p^4(^3P)3p$	$2s^22p^4(^3P)3d$	$^2D^o - ^4F$	5/2 – 7/2
Ne II 321.432	M	52.522	56.378	$2s^22p^4(^3P)3p$	$2s^22p^4(^3P)3d$	$^4D^o - ^4F$	3/2 – 5/2
Ne II 321.373	M	52.540	56.396	$2s^22p^4(^3P)3p$	$2s^22p^4(^3P)3d$	$^4D^o - ^4F$	1/2 – 3/2
Ne II 338.842	M	52.748	56.406	$2s^22p^4(^3P)3p$	$2s^22p^4(^3P)3d$	$^2D^o - ^2F$	3/2 – 5/2
Ne II lines in Group E presented in Fig. 9							
Ne II 421.974	M	56.172	59.110	$2s^22p^4(^3P)3d$	$2s^22p^4(^3P_2)4f$	$^4D - ^2[4]^o$	7/2 – 9/2
Ne II 439.199	M	56.301	59.123	$2s^22p^4(^3P)3d$	$2s^22p^4(^3P_2)4f$	$^4F - ^2[5]^o$	9/2 – 11/2
Ne II 440.930	M	56.312	59.123	$2s^22p^4(^3P)3d$	$2s^22p^4(^3P_2)4f$	$^2F - ^2[5]^o$	7/2 – 9/2
Ne II 437.955	M	56.366	59.196	$2s^22p^4(^3P)3d$	$2s^22p^4(^3P_1)4f$	$^4F - ^2[4]^o$	7/2 – 9/2

Note: all the values of the excitation energy of ionic lines given are the total excitation energy from the ground state of the atom (*i.e.* excitation energy + ionization energy).

*** *I* is the observed line intensity in pure neon plasma; VS= very strong; S= strong; M= medium and W= weak.**

**** *k* is for upper state and *i* is for lower state.**